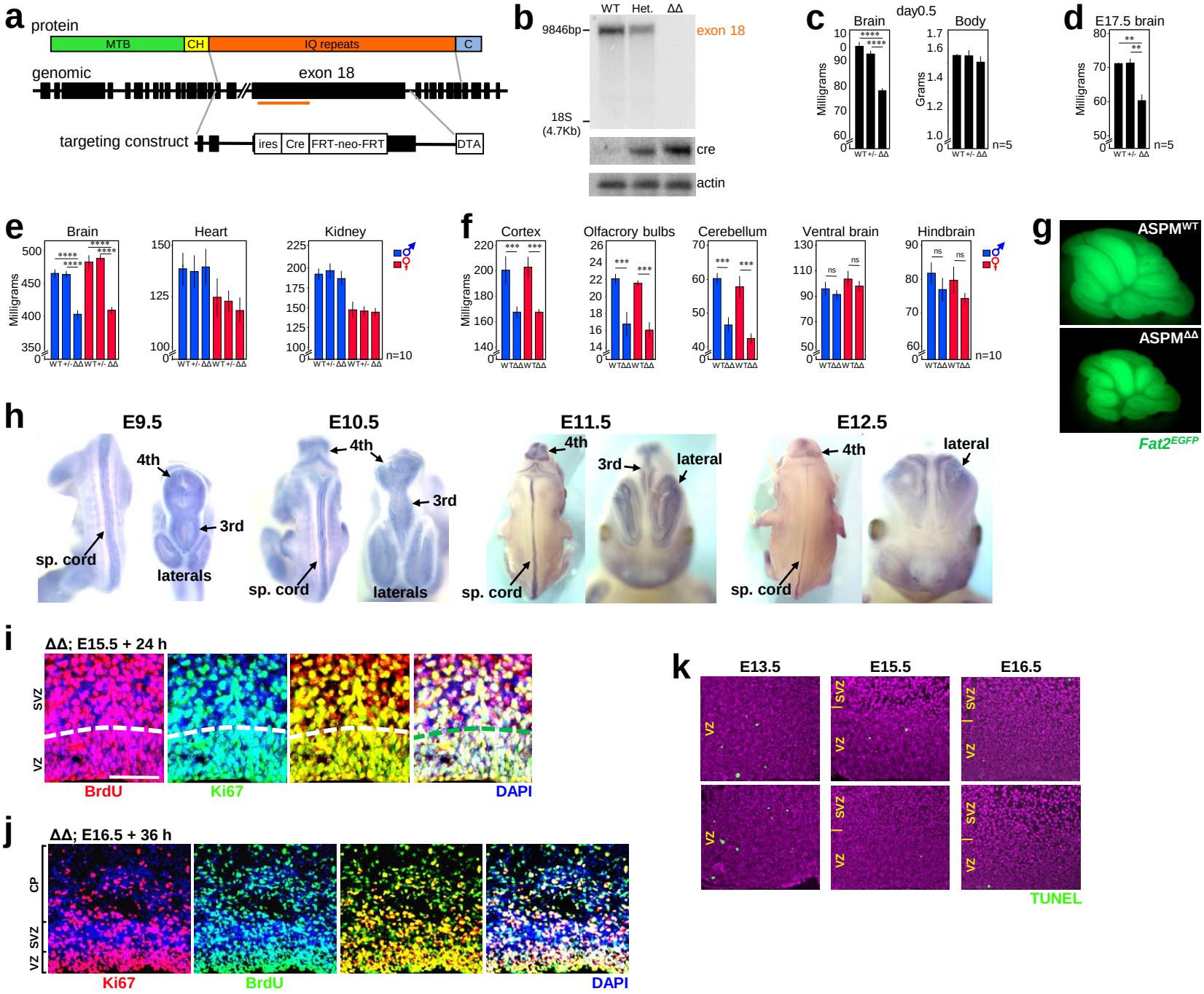
a
protein
MTB
CH
IQ repeats
C
genomic
exon 18
targeting construct
ires
Cre
FRT-neo-FRT
DTA
b
WT
Het.
ΔΔ
9846bp
exon 18
18S
(4.7Kb)
cre
actin
c
day0.5
Brain
Body
Milligrams
Grams
n=5
d
E17.5 brain
Milligrams
n=5
e
Brain
Heart
Kidney
Milligrams
n=10
f
Cortex
Olfacrory bulbs
Cerebellum
Ventral brain
Hindbrain
Milligrams
n=10
g
ASPM^WT
ASPM^ΔΔ
Fat2^EGFP
h
E9.5
E10.5
E11.5
E12.5
4th
3rd
lateral
laterals
sp. cord
i
ΔΔ; E15.5 + 24 h
SVZ
VZ
BrdU
Ki67
DAPI
j
ΔΔ; E16.5 + 36 h
CP
SVZ
VZ
Ki67
BrdU
DAPI
k
E13.5
E15.5
E16.5
VZ
SVZ
TUNEL

Supplementary Figure 1. (a) Scheme of *ASPM* genomic organization. Putative protein functional domains as well as coding exons are presented. To generate the *ASPM* mutant mouse, the majority of exon 18 was replaced via homologous recombination with an iresCre cassette followed by *CAG*-driven FRT-flanked *neo* gene. Splicing sites remained intact. Consequently, the mutant ASPM protein lacks the terminal 1717 amino acids containing the calmodulin binding domain and the C-terminus. This strategy generates truncated ASPM protein that represents the median size of all known human microcephaly associated mutations. 34 of 79 known human truncated ASPM proteins are due to mutations located before exon 18 that lead to premature termination codons[1, 2]. Accordingly, the deletion of a 2.6 kb genomic region of exon 18 yielded a nonsense mutation resulting in a bicistronic mRNA product containing ASPM protein truncated at amino acid 1405, and ires-derived Cre expression. The region within exon 18 used for *in-situ* hybridization and Northern blotting is indicated (orange bar). MTB, microtubule binding domain; CH, calponin binding domain; IQ, calmodulin binding domain; CTR, C-terminus; DTA, diphtheria toxin fragment A.
(b) Northern blot analysis of RNA from cortices of WT, heterozygous and $ASPM^{\Delta}$ mice confirms ablation of *ASPM* mRNA expression and emergent *CRE* expression. Western blot analyses confirming the predicted truncation of ASPM protein in homozygous mutant mice are shown in Figure 9b.
(c) Brain and body weight of $ASPM^{\Delta}$ pups and their WT and heterozygous littermates 12 h after birth, illustrating that the $ASPM^{\Delta}$ brain is significantly lighter in total wet weight. In contrast, there is no significant difference in body weight.
(d) Average brain weights of E17.5 $ASPM^{\Delta}$ embryos and their WT and heterozygous littermates shows that even at embryonic stages the $ASPM^{\Delta}$ total wet weight brain is significantly lighter.
(e) Average gender specific brain weights of adult $ASPM^{\Delta}$ mice and their WT and heterozygous littermates at 10 weeks, which shows that the $ASPM^{\Delta}$ total wet brain weight is significantly lighter irrespective of sex. In contrast, no significant differences were evident in wet weight comparisons of two other internal organs.
(f) Adult mouse brains were separated into five major brain structures and the weight of each part is presented. In $ASPM^{\Delta}$ mice the weight of the cerebral cortex, olfactory bulbs and cerebellum structures are significantly reduced, whereas the ventral brain and hindbrain are only slightly reduced. Ventral brain includes the basal ganglia, ventricles, thalamus, hippocampus and the paleocortex.
(g) Sagittal view of $ASPM^{\Delta}$ and WT cerebella of littermates at 10 weeks labeled with EGFP within the expression domain of the protocadherin gene, *Fat2*[3].
(h) Expression of *ASPM* in mouse embryo shown by whole mounts *in situ* hybridization to antisense probe (Supplementary Figure 1a). Embryos at E9.5 to E12.5 exhibited progressively decreased *ASPM* expression, which ultimately intensified predominantly along the four ventricles of the developing CNS that maintain the ventricular and subventricular proliferative regions. Previously reported *in situ* hybridization analyses on E14.5 and E16.5 coronal cortical sections[4], E14 parasagital section[5], and IHC analysis on E15.5 cortical section[6] showed similar progressive decrease in *ASPM* expression with predominant appearance in the cerebral cortical VZ, the proliferative region of the medial and lateral ganglionic eminences, and the VZ of the dorsal diencephalon.

(i) Growth fraction (GF), defined as the proportion of cells that are actively proliferating, is taken to correspond to the maximum labeling index (LI) achieved in a given proliferative zone. It is determined by cumulative labeling till saturation of the cycling population with S-phase marker via a series of periodic injections, as previously described[7, 8]. E15.5 pregnant females were i.p. injected with BrdU (50 μg/gm body weight). Injections were repeated at 3 h intervals over a period of 24 h, which was sufficient to embrace the duration of the entire cell cycle of both *ASPM*$^{\Delta}$ and WT ventricle zone progenitors (Fig. 2d). The last BrdU injection was administrated 0.5 h before the dam was sacrificed. The GF of normal VZ was previously established to be uniformly near 1[5]. Likewise, GFs of *ASPM*$^{\Delta}$ VZ as well as that of WT littermates (not shown) were ~1, as cumulative BrdU administration over 24 h labeled nearly 100% of nuclei in the developing cortex. Empirical data showed that GFs measured by BrdU cumulative labeling and Ki67 are the same[9]. Accordingly, the GF for the *ASPM*$^{\Delta}$ VZ was further confirmed to be homogeneously practically 1, as virtually all the VZ progenitors were Ki67 positive. Dashed white and green lines indicate the border between cortical VZ and SVZ. The figures shown are representative of three repeated experiments.

(j) E16.5 pregnant females were used for the evaluation of GF of SVZ proliferating cells. Thirteen periodic BrdU injections were administrated to encompass the entire duration of cell cycle of both *ASPM*$^{\Delta}$ and WT SVZ progenitors (Fig. 2e). Labeling indexes for cortical layers outside of the VZ margin reaches the maximum value which is less than 1, due to the presence of two distinct nonproliferative cell types: postmitotic young neurons which exited S-phase just before the initial injection of BrdU and progenitor cells in G0. Accordingly, the fraction of cumulatively BrdU labeled cells in E16.5 + 36 h SVZ of *ASPM*$^{\Delta}$ (39% ± 0.4%) and WT (40% ± 0.5%, not shown) littermates was comparable. Of note, not all cumulatively BrdU labeled SVZ cells, over the period of 36 h, co-expressed Ki67 and vise versa; few Ki67-positive proliferating SVZ cells did not incorporate BrdU. Nevertheless, assessment of GF as the proportions of Ki67-positive cells produced comparable conclusion (*ASPM*$^{\Delta}$; 41% ± 1.4%, WT; 43% ± 0.9%). The figures shown are representative of three repeated experiments. CP, cortical plate.

(k) Matching coronal somatosensory cortical sections were processed for terminal deoxynucleotidyl transferase-mediated dUTP-biotin nick-end labeling (TUNEL-green), and were counterstained with DAPI (pseudo-purple). No significant differences in the proportions of TUNEL-positive cells were observed between *ASPM*$^{\Delta}$ and WT control littermates in both VZ and SVZ proliferative zones, accommodating typical <1% apoptotic event per cell cycle[10].

Data are represented as mean ± s.e.m. ** $P < 0.005$, *** $P < 0.0005$, **** $P < 0.0001$ by Student's *t*-test.

Scale bars, 100 μm.

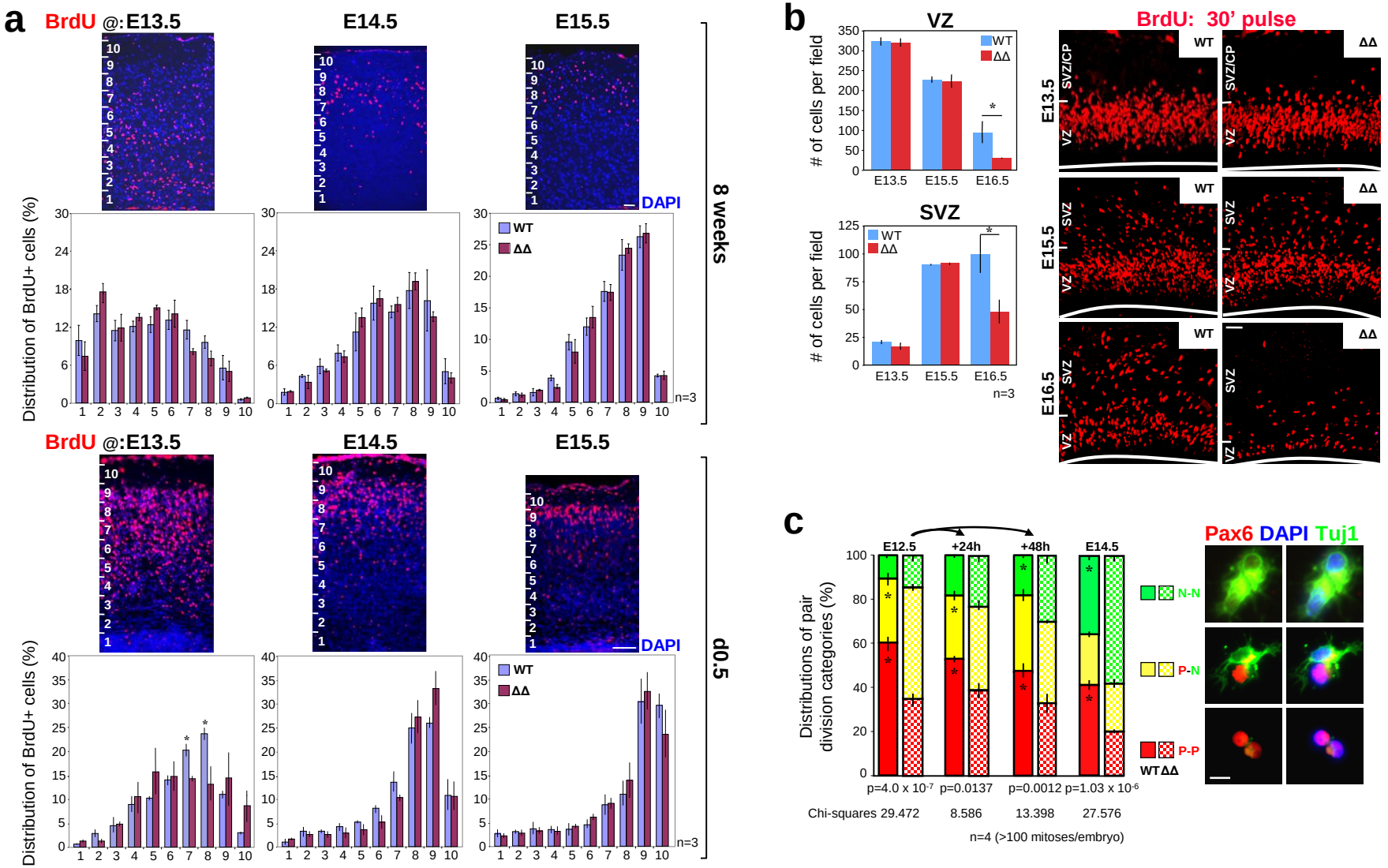

Supplementary Figure 2. ASPM is critical for maintenance of the VZ-NPC compartment and their balanced proliferative/neurogenic divisions, but not for neuronal migration.

(a) Since gross cortical patterning of neurons appears relatively normal in *ASPM*$^{\Delta}$ brains (Fig. 1e,f), neuronal migration is an unlikely etiology. Nevertheless, BrdU birthdating assay was carried out to study neural migration in *ASPM*$^{\Delta}$. Pregnant females were singly injected intraperitoneally with BrdU at E13.5, E14.5, and E15.5. The offspring were analyzed the morning after birth or eight weeks postnatal for BrdU-positive neurons in their cerebral cortices.

Matching coronal somatosensory cortical sections of *ASPM*$^{\Delta}$ and their WT littermates were each divided into ten equal bins from the ventricle to the pial surface, and the number of BrdU-labeled neurons in each bin was counted. Since fewer BrdU-positive neurons were observed in *ASPM*$^{\Delta}$ brains, especially when BrdU was administrated at later stage of cotricogenesis (E15.5), the distribution of the BrdU-positive cells relative to the distance from the ventricular surface was plotted as percentages of overall positive cells in the field. Neurons labeled at later stages of corticogenesis (E14.5 and E15.5) showed mostly an outer layers distribution that was indistinguishable between *ASPM*$^{\Delta}$ and WT. The distribution of *ASPM*$^{\Delta}$ neurons labeled at E13.5 differs significantly at d0.5 ($P = 0.026$, Chi-square test). On the other hand, distribution of E13.5 labeled *ASPM*$^{\Delta}$ neurons in their final, predominantly deeper layers position (week 8), resembles WT neurons ($P = 0.877$, Chi-square test). The figures shown are representative of three brains from *ASPM*$^{\Delta}$ mutant mice and their WT littermates from two different litters analyzed at each time point. Chi-squares (degrees of freedom 9): BrdU @ E14.5, assayed @ d0.5 $P = 0.742$. BrdU @ E14.5, assayed @ week 8 $P = 0.995$. BrdU @ E15.5, assayed @ d0.5 $P = 0.970$. BrdU @ E15.5, assayed @ week 8 $P = 0.994$. These data rule out deficiency in neural migration as likely cause for the *ASPM*$^{\Delta}$ cortical hypoplasia. The slow or delayed early (E13.5) migrating neurons observed in d0.5 mutant eventually migrate to appropriate cortical layers, suggesting that the transient setback was due to hindered cell cycle exit of progenitors. However, it does not rule out the possibility of an unusual transient migration defects that are compensated for at later developmental stages.

(b) Premature exhaustion of the NPC compartment in *ASPM*$^{\Delta}$ embryos. Embryos were pulse labeled for 30 minutes by intraperitoneal BrdU injections to pregnant females. Matching coronal somatosensory cortical sections were stained with anti-BrdU antibody. Approximately equal numbers of BrdU-labeled progenitors were observed in *ASPM*$^{\Delta}$ and WT littermate cortices in both VZ and SVZ proliferative regions at E13.5 and E15.5. At E16.5, on the other hand, strikingly fewer BrdU-labeled cells were seen in *ASPM*$^{\Delta}$ cortex in both proliferative zones, indicating that ASPM deficiency leads to depletion of cortical progenitor pool at late corticogenesis. White lines indicate the position of cortical ventricular surface. Cell counts were performed manually in a fixed area of 500 μm (medial-lateral) and 6 μm thick (rostral-caudal) for the two different zones of the embryonic cortex.

(c) Enhanced pair cell assay (corresponding to Fig. 1j). In order to eliminate traces of orientation-dependent signals transferred during isolation of NPC, the proportions of division events were measured in paired cell-siblings that underwent one or two *ex vivo* divisions. Once again, *ASPM*$^{\Delta}$ cells completed considerably more neurogenic P–N and N-N divisions. *ASPM*$^{\Delta}$ cells that underwent one *ex vivo* division (E12.5 + 24 h) completed considerably more P–N divisions, in proportions similar to freshly isolated E12.5 NPC. Cells that underwent two *ex vivo* divisions (E12.5 + 48 h) carried out significantly more terminal N-N divisions; a tendency exhibited by freshly isolated E14.5 NPC. Chi-squared statistical analyses show that distribution of *ASPM*$^{\Delta}$ mode of division is significantly different than control.

Data are represented as mean ± s.e.m. * $P < 0.05$, by Student's *t*-test. Scale bars, 20 μm (c), 50 μm (a, b).

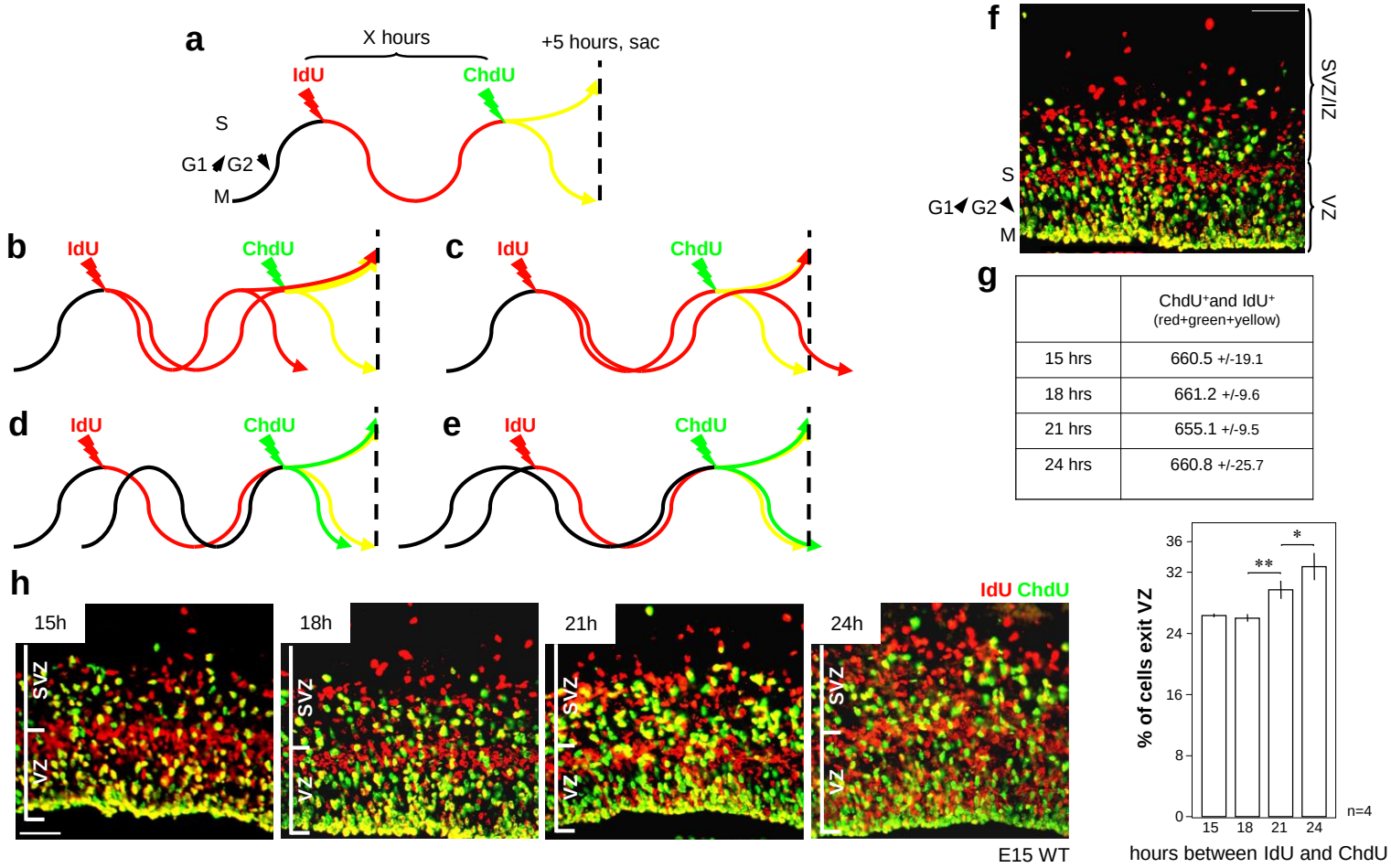

	ChdU+and IdU+ (red+green+yellow)
15 hrs	660.5 +/-19.1
18 hrs	661.2 +/-9.6
21 hrs	655.1 +/-9.5
24 hrs	660.8 +/-25.7

Supplementary Figure 3. Direct demonstration of the association between cell-cycle duration and NPC tendency to leave the VZ. Previous studies demonstrating the link between C.C. duration and mode of division have relied on artificial protocols that selectively modify the efficiency of G1 progression[11-17]. To establish the certainty of a relationship between C.C. length and propensity to exit the VZ, we employed an *in vivo* double S-phase-labeling procedure.

(a-e) Schematic outline of the IdU/ChdU double-S-phase labeling paradigm. Iododeoxyuridine (IdU) was administrated as a single i.p. injection to WT pregnant dams carrying E15 embryos. It was followed by a second single i.p. injection of chlorodeoxyuridine (ChdU) 15, 18, 21 and 24 h later. Mice were sacrificed 5 h later corresponding to a time interval adequate for the cells to execute their decision to exit the VZ or re-enter S-phase in order to continue proliferate in the VZ. This design identifies a cohort of progenitor cells that were at S-phase during the first injection of IdU (red), and whose cell cycle duration was equal to the experimental 'X' hours. Thus, they reached S-phase once again when the second injection of ChdU (green) was administrated (a) and appeared yellow.

Therefore, only these double-labeled yellow nuclei were counted for each time period. Cells that were at S-phase during the first injection (IdU) but their cell cycle duration was shorter (b) or longer (c) then the experimental 'X' hours, were not in S-phase during the second injection (ChdU), therefore appeared as red nuclei and were not counted. Conversely, cells that were not at S-phase during the first injection (IdU) and their cell cycle duration is shorter (d) or longer (e) then the experimental 'X' hours therefore happened to be in S-phase during the second injection (ChdU) appeared as green nuclei, and were ignored as well.

(f) The S-phase zone, that is, the outer VZ toward the ventricular margin[8] served as an approximate border between the VZ and SVZ. It thoroughly corresponded with the dense pseudostratified appearance of the neuroepithelial VZ-NPC.

(g) Analyses were performed on coronal sections taken from approximately the mid-hemisphere level corresponding to the primordial primary somatosensory cortex. Total cell counts in a fixed area of 500 μm in its medial-lateral dimension and 6 μm (corresponding to section thickness) in its rostral-caudal dimension shows roughly equivalent numbers regardless of the duration of the experiments. Therefore, within the 9 h gap (E15.5+15 h to E15.5+24 h) comparatively similar number of Medial Ganglionic Eminence (MGE) cells invades the SVZ and IZ. Thus, such cells do not have an effect on the paradigm accuracy.

(h) Yellow nuclei above the S-phase zone were considered as fraction of cells that exit the VZ, while yellow nuclei within and below the S-phase zone were considered as VZ-NPC. Data represented as double-stained IdU^+ChdU^+ (yellow) nuclei above the S-phase zone as percentage of total IdU^+ChdU^+ cells in the field. Results show that WT E15 precursors with a C.C. exceeding a threshold of 18 h are more likely to exit the VZ progenitor pool in a duration-dependent manner, indicating an *in vivo* predisposition of longer cycling NPC to advance to the next corticogenesis step. In contrast, VZ-NPC whose C.C. was faster than the given threshold were indifferent to its duration. Thus, fate decision of faster proliferating cells appears to correlate with the cleavage plane orientation, previously shown to play pivotal role during early stages of corticogenesis[10].

* $P < 0.05$, ** $P < 0.005$, by Student's *t* test. Scale bars represent 50 μm.

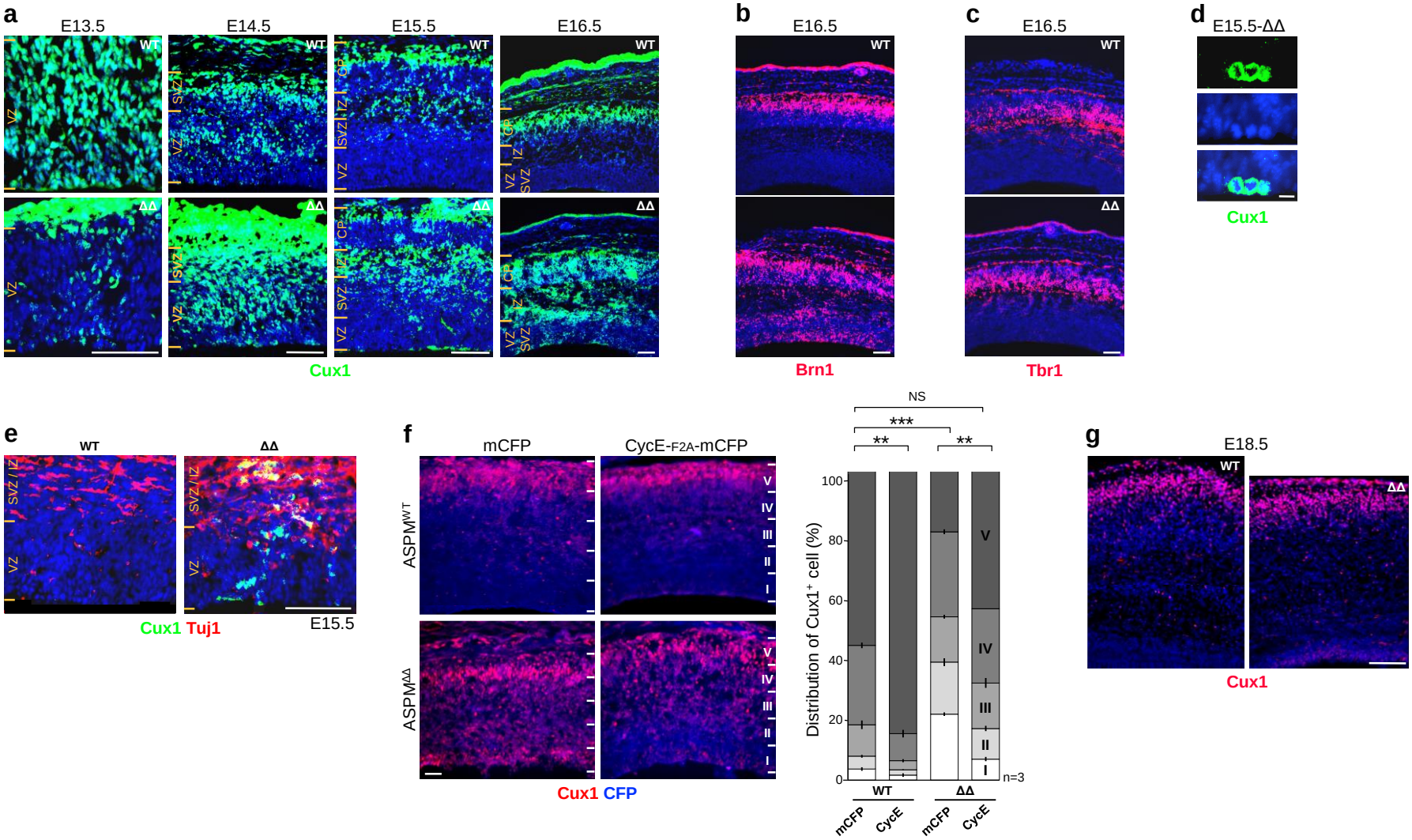

Supplementary Figure 4. *ASPM*$^{\Delta}$ NPC exhibited delayed succession of an internal clockwise developmental sequence.
(a) Matching embryonic coronal somatosensory cortical sections of *ASPM*$^{\Delta}$ and WT littermate stained for Cux1. Expression and cellular localization of the *Cux1* and *Brn1* transcription factors (genes that regulate the maturation and fate of later born neurons[18, 19]) follows a defined sequential pattern during corticogenesis. At E13.5 WT NPC exhibited diffuse cytoplasmic and nuclear Cux1 immunoreactivity throughout the entire VZ while *ASPM*$^{\Delta}$ NPC displayed scarce Cux1 expression. Widespread Cux1 expression was first observed in E14.5 *ASPM*$^{\Delta}$ cortical NPC (nuclear, cytoplasmic and mitotic). At E15.5, a large number of Cux1^{+} WT neurons destined to the cortical upper layers, were observed migrating away from the proliferative zones through the intermediate zone (IZ) and the cortical plate (CP), while none were detected in the VZ.

From this point forward, immunoreactivity is strictly nuclear. However, behind schedule Cux1$^+$ cells were still located within the VZ and SVZ of mutant cortex, some of which were basal mitoses with intense cytoplasmic Cux1 (e). By E16.5, all WT Cux1$^+$ neurons have reached their final supragranular destination, while most of *ASPM*$^\Delta$ Cux1$^+$ cells were still migrating through the IZ and CP, and a few were yet residing in the VZ.

(b) Matching embryonic coronal somatosensory cortical sections of *ASPM*$^\Delta$ and WT littermate stained for Brn1 at E16.5. Similar to Cux1 all WT Brn1$^+$ neurons have reached their final destination at layers II-IV, while most of *ASPM*$^\Delta$ Brn1$^+$ cells were still migrating through the IZ and CP, and a few were yet residing in the VZ.

(c) Spreading of *ASPM*$^\Delta$ NPC destined for deep cortical layers, marked by *Tbr1*[20], was normal.

(d) High-magnification of *ASPM*$^\Delta$ E15.5 coronal cortical section showing high resolution of basal mitoses stained for Cux1. The behindhand cytoplasmic presence of Cux1 is another feature of inappropriate maturation of supragranular layers II/III- and IV, indicative of impaired proliferation rhythm of *ASPM*$^\Delta$ NPC.

(e) Matching E15.5 coronal somatosensory cortical sections of *ASPM*$^\Delta$ and WT littermate stained for Cux1 and the neuronal marker-Tuj1, verifying that the uncharacteristically positioned Cux1 positive *ASPM*$^\Delta$ NPC were not impeded differentiated cells, as they lacked Tuj1 expression.

(f) The delayed sequence of cortical development within *ASPM*$^\Delta$ cortices is Cyclin E-dependent. Cux1 stained E16.5 coronal cortical sections 48 h following lentiviral-Cyclin E transduction, each divided into five equal bins from the ventricle to the pial surface. The number of Cux1$^+$ cells in each bin was counted and distribution of positive cells relative to the distance from the ventricular surface was plotted as percentages of overall positive cells in the field. Chi-squared statistical analysis confirmed that distribution of Cux1$^+$ cells differs significantly between *ASPM*$^\Delta$ and WT. Delayed corticogenesis was rescued, as Cux1 distribution along Cyclin E transduced *ASPM*$^\Delta$ cortices doesn't differ significantly from control mCFP treated WT controls. Notably, Cux1 distribution along Cyclin E transduced WT cortices was significantly different than mCFP treated WT controls, demonstrating more peripheral positioning. ** $P < 0.005$, *** $P < 0.0001$, by Student's *t* test.

(g) By E18.5, as embryonic corticogenesis ceases, the behindhand *ASPM*$^\Delta$ Cux1$^+$ cells have finally reached their prospective destination in layers II-IV.

Scale bars represent 10 μm (d), 50 μm (f), 100 μm (a, b, c, e), 500 μm (g).

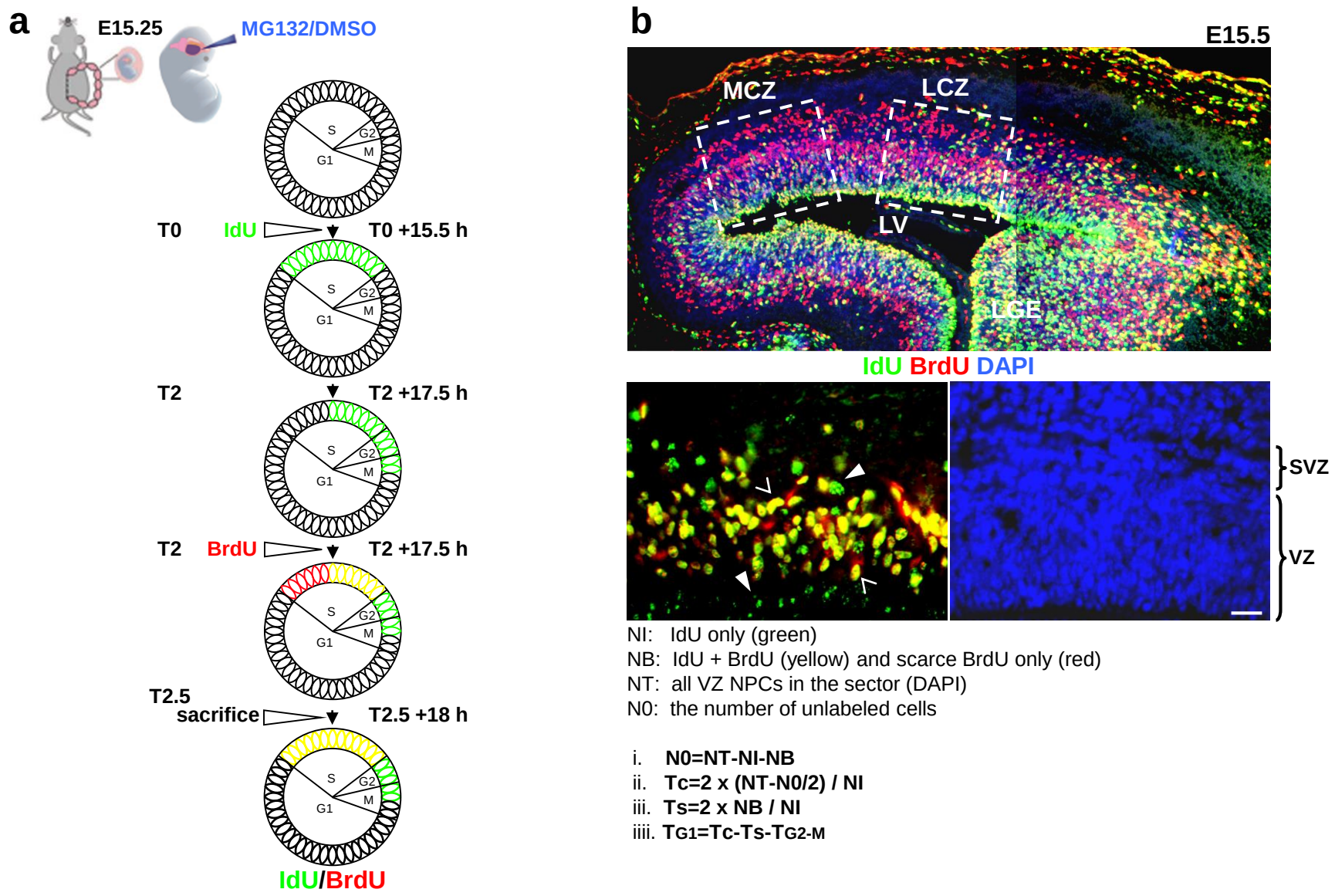

Supplementary Figure 5 (a) Experimental design of the double S-phase labeling paradigm for the estimation of cell cycle parameters according to[21, 22]. IdU was administrated by a single i.p. injection to pregnant females (T0), followed by a single injection of BrdU 2 h later (T2). Mice were sacrificed after half an hour (T2.5). IdU- and BrdU- labeled cells were stained green and red, respectively therefore three types of labeled cells were expected. Cells that were within S-phase at T0-T2 and then proceeded to G2/M-phase at T2–T2.5 should be IdU labeled only- green. Cells entering S-phase at T2–T2.5 should be BrdU labeled only- red. Cells within S-phase at both T0 and T2 were IdU/BrdU co-labeled- yellow.

However, due to the nonspecific detection of the anti-IdU antibody for both IdU and BrdU, red-labeled cell were not noticeable. Thus, only two cell types can be reliably distinguished and counted. These are IdU-only green labeled cells, which were in S-phase at the time of the IdU injection and exited the S-phase by the time of the BrdU injection, and yellow labeled cells that are both BrdU-only labeled and IdU/BrdU-double labeled. The cells that were not labeled with either IdU or BrdU were not in S-phase when effective labeling concentrations of either tracer were available. For measurements of cell cycle parameters following *in utero* administration of the proteosome inhibitor (Fig. 7d,e), MG132 or DMSO were injected at E15.25. T0 was 15.5 h later and the entire double S-phase labeling procedure was carried out within 18 h.

(b) A representative coronal section taken from approximately the mid-hemisphere level corresponding to the primordial primary somatosensory cortex of E15.5 embryo stained for IdU (green), BrdU (red) and DAPI (blue). Bearing in mind that the neurogenetic schedule of progenitors in the LCZ is developmentally 'in advance' of those in the MCZ by at least 24 h[22, 23], analyses were performed at two locations along the medial-lateral axis of the VZ. LCZ- and MCZ, lateral and medial cortical zones, respectively; LV: lateral ventricle. A representative higher magnification view of a cortical sector, which allows detection of the expected two cell types, is also shown. The IdU-only labeled cells are green (solid arrowheads) and IdU/BrdU-double labeled cells are yellow (open arrowheads). Scale bar represents 50 μm.
To measure the cell cycle (T_C) and the S-phase (T_S) durations, three types of cells in a fixed area of 500 μm (medial-lateral) and 6 μm thick (rostral-caudal) were counted:

a; IdU-only labeled cells- NI.
b; scarce BrdU-only and BrdU/IdU double-labeled cells- NB.
c; all DAPI labeled cells in the VZ within the field- NT.

The number of unlabeled cells (N0) was taken by subtracting IdU and/or BrdU labeled cells from the total (Supplementary Table 1).

i. $N0=NT-NI-NB$

The kinetic parameters, T_C and T_S, were derived according to the double-labeling algorithm formulation in[22], according to the following equations:

ii. $T_C = 2 \times (NT-N0/2) / NI$
iii. $T_S = 2 \times NB / NI$

Following assessment of the time-span for passing through G2- and M- phases using the PLM method (see Supplementary Figure 8), the length of T_{G1} was calculated by subtracting T_S and T_{G2-M} from T_C:

iiii. $T_{G1} = T_C - T_S - T_{G2-M}$

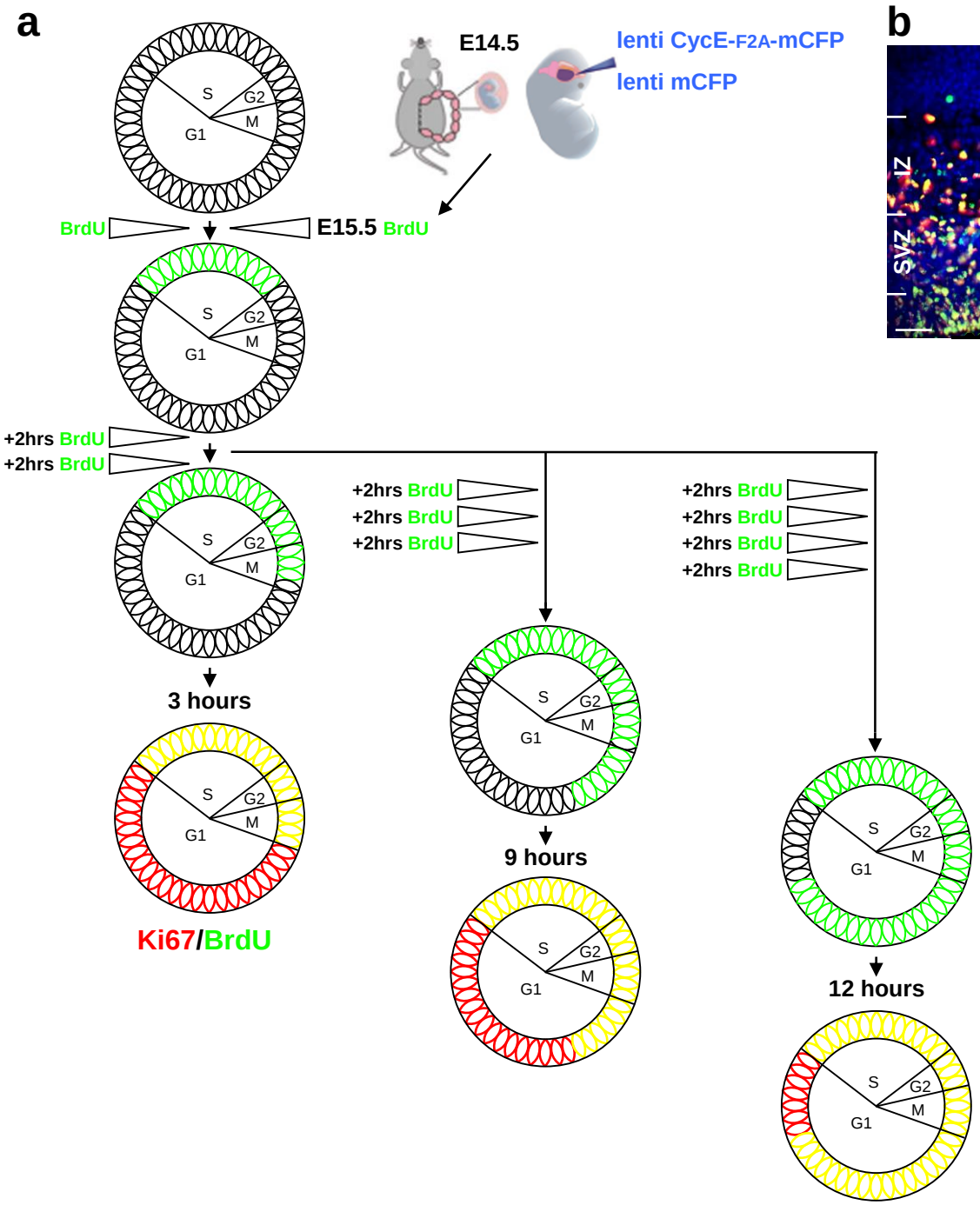
a
S
G2
M
G1
E14.5
lenti CycE-F2A-mCFP
lenti mCFP
BrdU
E15.5 BrdU
+2hrs BrdU
+2hrs BrdU
3 hours
Ki67/BrdU
+2hrs BrdU
+2hrs BrdU
+2hrs BrdU
9 hours
+2hrs BrdU
+2hrs BrdU
+2hrs BrdU
+2hrs BrdU
12 hours

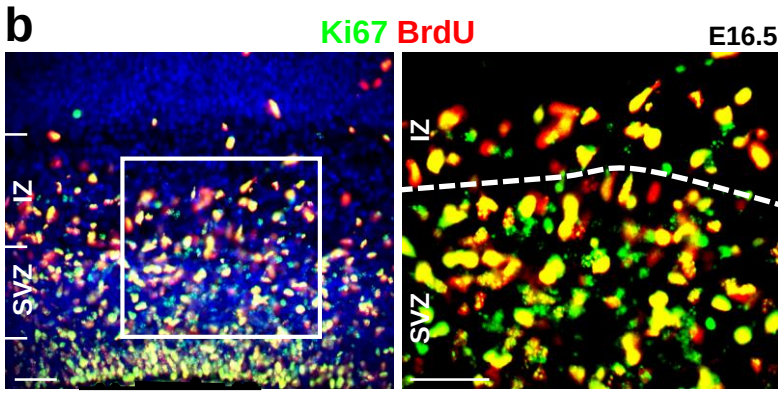
b
Ki67 BrdU
E16.5
IZ
SVZ
IZ
SVZ

Supplementary Figure 6 (a) Experimental design of the cumulative BrdU labeling for determination of T_C and T_S. Cell cycle (T_C) and S-phase (T_S) durations were determined according to published protocols[8, 23, 24]. For SVZ measurements E16.5 dams were i.p. injected with BrdU. Subsequent injections were performed at intervals of 2 h, with a final BrdU injection 0.5 h prior to termination. Embryos were collected at 4 survival points, 3, 9, 12, and 36 h after the initial injection. LI (labeling index) was defined as the proportion of labeled cells ($BrdU^+$) to total proliferating ($Ki67^+$) cells. For each group, a least-square curve fit that considered all data points from every survival time was generated using Microsoft (Seattle, WA) Excel (Fig. 2e). T_C and T_S were determined according to following equations:

i. $T_C = 1/\text{slope}$
ii. $T_{LI=100\%} = T_C - T_S$ (that is the extrapolated intercept of the LI = 0 on the x-axis)

For measurements of cell cycle parameters following *in utero* lentiviral-Cyclin E transduction (Fig. 5g), viral particles were injected at E14.5. Labeling began 24 h later.

(b) A representative coronal section taken from approximately the mid-hemisphere level corresponding to the primordial primary somatosensory cortex of E16.5 embryo, stained for Ki67 (green), BrdU (red) and DAPI (blue) for estimation of the *in vivo* duration of T_C and T_S in SVZ-NPC by cumulative BrdU labeling.
Scale bars represent 20 μm.

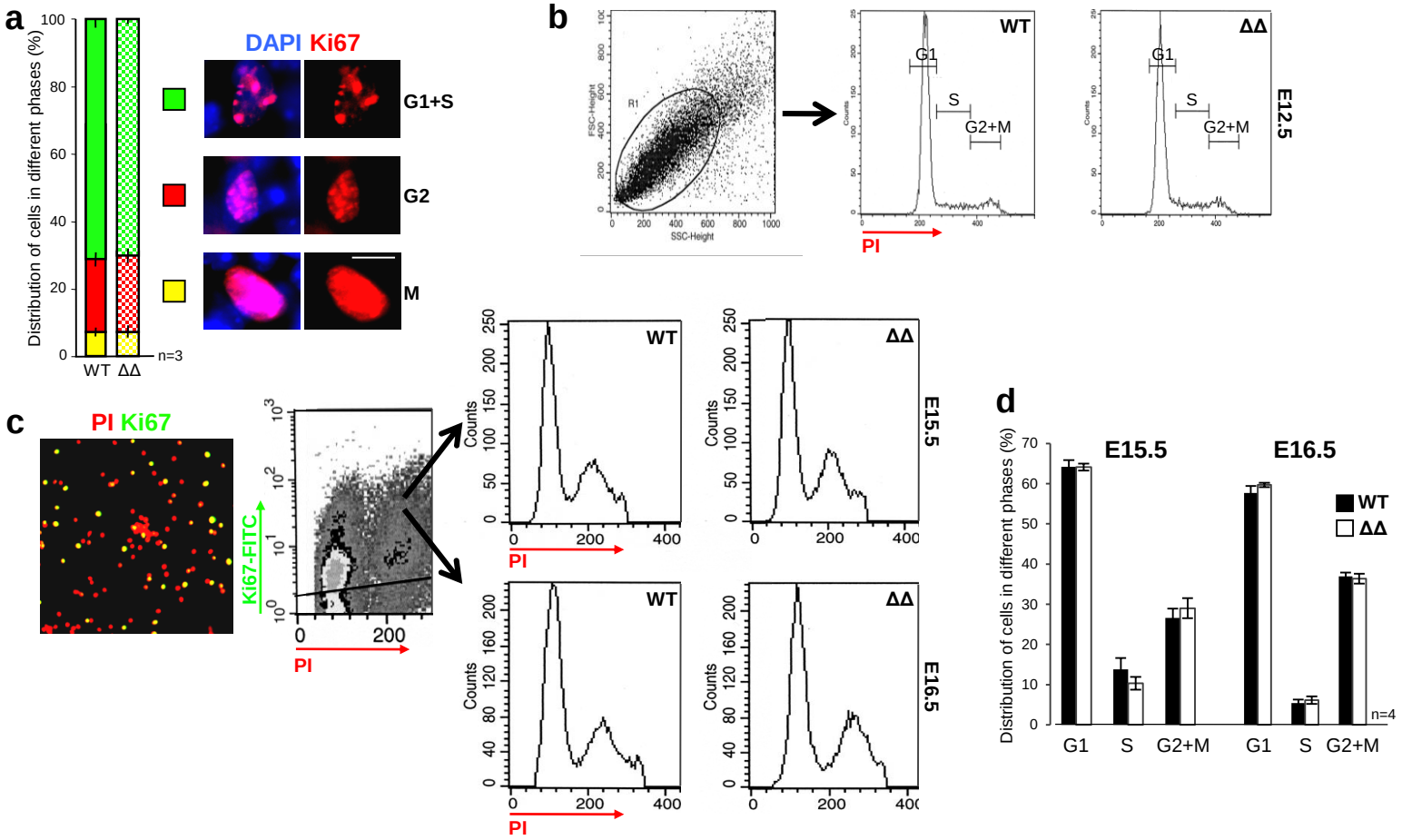

Supplementary Figure 7. Normal distribution of *ASPM*$^{\Delta}$ cell cycle phases. **(a)** Taking advantage of qualitative differences in Ki67 staining within cell cycle phases. Comparable proportions of NPC exhibiting sparse punctuate staining (G1+S phases), dense punctuate staining (G2 phase), and dense uniform staining (M phase) of Ki67 were evident in *ASPM*$^{\Delta}$ and WT E15.5 cerebral cortices. Data points represent mean ± s.e.m. Not significant by Student's *t* test. Scale bar represents 10 µm.

(b-c) Quantification of NPC distribution across different cell cycle phases based on FACS analysis. Cell sorting was performed on dissociated cells taken from E12.5, E15.5 or E16.5 *ASPM*$^{\Delta}$ and WT telencephalic lobes. The single cell suspensions were treated with propidium iodide (PI) to stain the DNA and generate histograms of DNA content, indicative of the cell cycle phase. At E12.5 (b) the cerebral wall consists primarily of VZ-NPC and the beginnings of a primitive plexiform zone[8]. Cells isolated from older embryos were a combination of progenitors and differentiated neurons. Hence, only the proliferating Ki67^{+} fraction of cells were analyzed and its DNA content was plotted (c).

(d) Data points represent mean ± s.e.m. Not significant by Student's *t* test

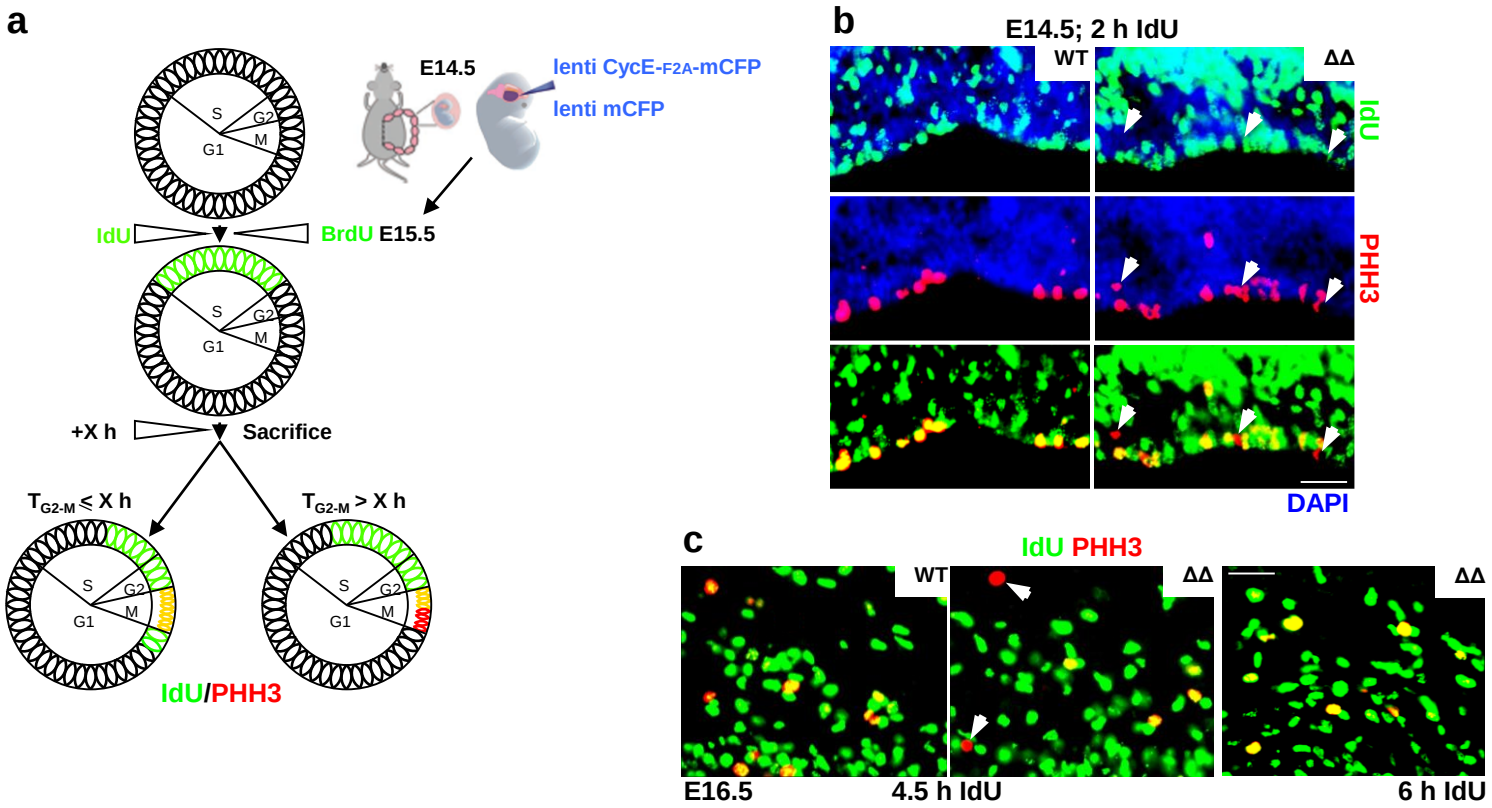

Supplementary Figure 8. Experimental design principles of PLM (percentage of labeled mitotic figures) procedure according to[25].
(a) The procedure is based on a brief exposure of cells to IdU by a single i.p. injection with embryos harvested at increasing intervals. The time interval (X) required for 100% IdU labeling of cells positive for the mitotic marker phosphohistone H3 (PHH3) corresponds to the time needed for the progress through G2 and M phases. That is, in case of $T_{G2\text{-}M} \leq$ (X) h, all $PHH3^+$ cells should be yellow whereas if $T_{G2\text{-}M} >$ (X) h, some $PHH3^+$ cells would be red. Mitotic figures were considered to belong to the VZ only if they were adjacent to the ventricular surface. For estimation of $T_{G2\text{-}M}$ following *in utero* lentiviral Cyclin E transduction (Fig. 5), viral particles were injected at E14.5. IdU labeling began 24 h later.
(b) Representative E14.5 coronal cortical sections stained for IdU and PHH3 for the evaluation of the VZ-PLM values (T_{G2+M}). Nearly 100% of WT mitotic $PHH3^+$ VZ-NPC were IdU labeled by 2 h post-injection. Conversely, the PLM of *ASPM*$^{\Delta}$ VZ-NPC reached roughly 100% only after ~3.5 h (not show) (Supplementary Table 3).
(c) Representative E16.5 coronal cortical sections stained for IdU and PHH3 for the evaluation of SVZ-PLM values (T_{G2+M}). Among WT SVZ-NPC 100% IdU labeling of mitotic $PHH3^+$ cells occurred 4.5 h post-injection, but only after 6 h in *ASPM*$^{\Delta}$ mitoses (Supplementary Table 4).
Scale bars represent 50 μm.

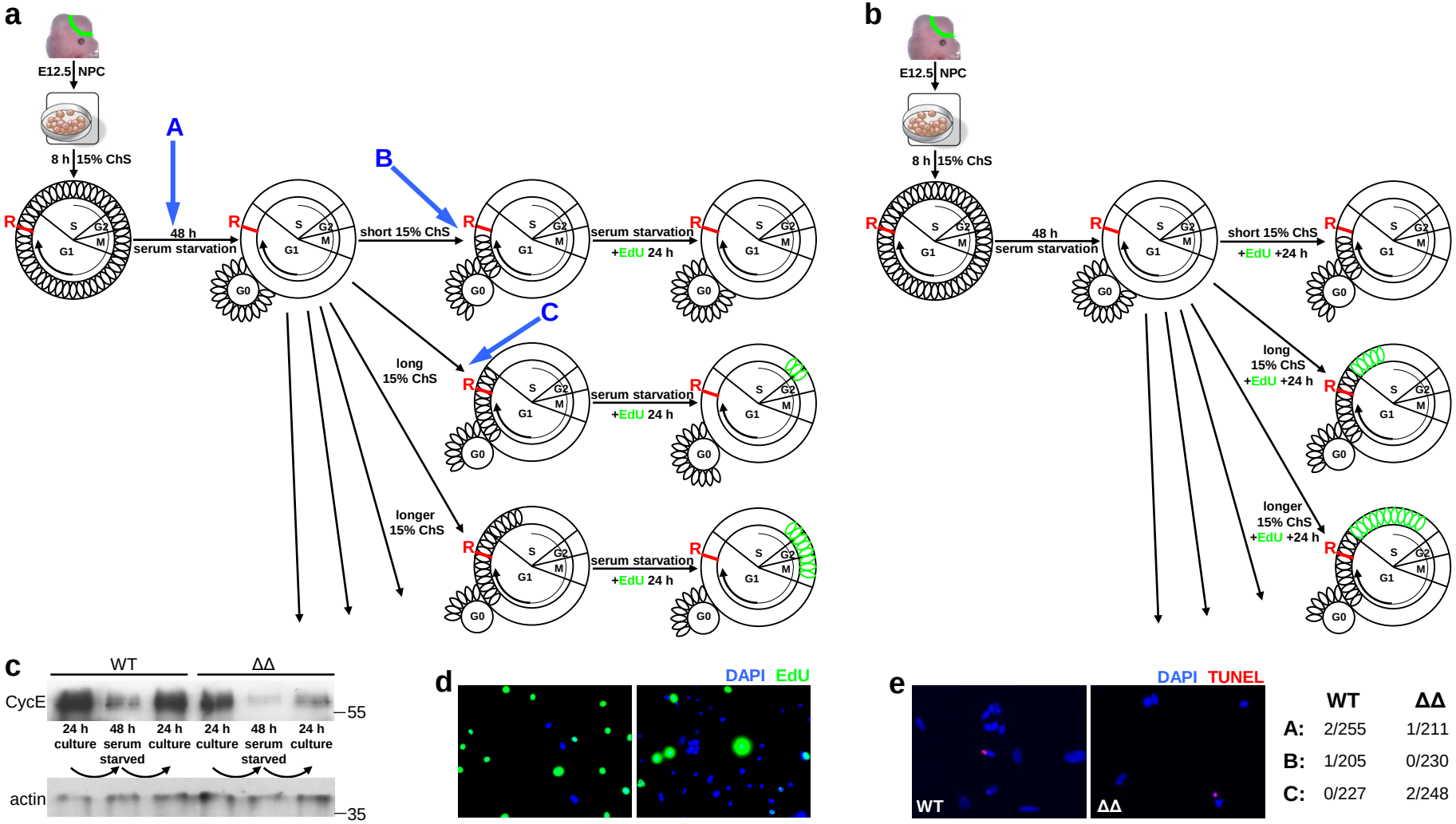

Supplementary Figure 9. Experimental design principles for determination of the restriction point.
(a) To assess the R-point along the G_0-to-S interval, E12.5 telencephalic NPC were isolated and allowed to attach for 8 h in neurospheres medium containing 15% chicken serum (ChS) and bFGF. Subsequently, cells were serum starved for 48 h in medium containing 0.25% ChS (+bFGF) and synchronized in G_0. To initiate cell cycle entry, 15% ChS-supplemented medium was re-applied, and later was switched to serum-free medium containing EdU tracer at successive time points. The experiment was terminated after 24 h and proportions of EdU labeled cells (relative to total DAPI-stained nuclei) were determined using the Click-iT EdU imaging kit, and plotted against time of ChS stimulation (Fig. 2g). The half point in which 50% of cells have transferred to serum/growth factors independence is considered as average early-G1-duration.

(b) Experimental design principles for determination of G1-phase duration. Synchronized NPC that had been deprived of serum for 48 h received 15% ChS-supplemented medium containing EdU. S-phase entry was determined at successive time points as above (Fig. 2h). Note, similar kinetics between *ASPM*$^{\Delta}$ and WT confirm that mutant G_0 NPC reinstate C.C. at the same rate as WT.
(c) Protein lysates of E12.5 telencephalic NPC were analyzed for Cyclin E expression by Western blotting. Cells were cultured for 24 h in regular 15% ChS plus bFGF supplemented medium. Aliquot of cells were serum starved for 48 h. Aliquot of starved cells were re-cultured in 15% ChS plus bFGF supplemented medium. Equivalent kinetics of reinstatement of Cyclin E expression between *ASPM*$^{\Delta}$ and WT indicate that mutant G_0 NPC reinstate C.C. at the same rate as WT.
(d) Representative fields showing EdU labeled NPC.
(e) NPC synchronized in G_0 ((A) in the experimental design scheme) and after short (B) or long (C) exposure to serum were processed for terminal deoxynucleotidyl transferase-mediated dUTP-biotin nick-end labeling (TUNEL-red). No significant differences in the proportions of apoptotic cells were observed between *ASPM*$^{\Delta}$ and WT NPC. Collectively, the absence of cell death and the control experiment shown in Supplementary Figure 9c prove that *ASPM*$^{\Delta}$ NPC do not endure decreased health or increased serum-dependency.

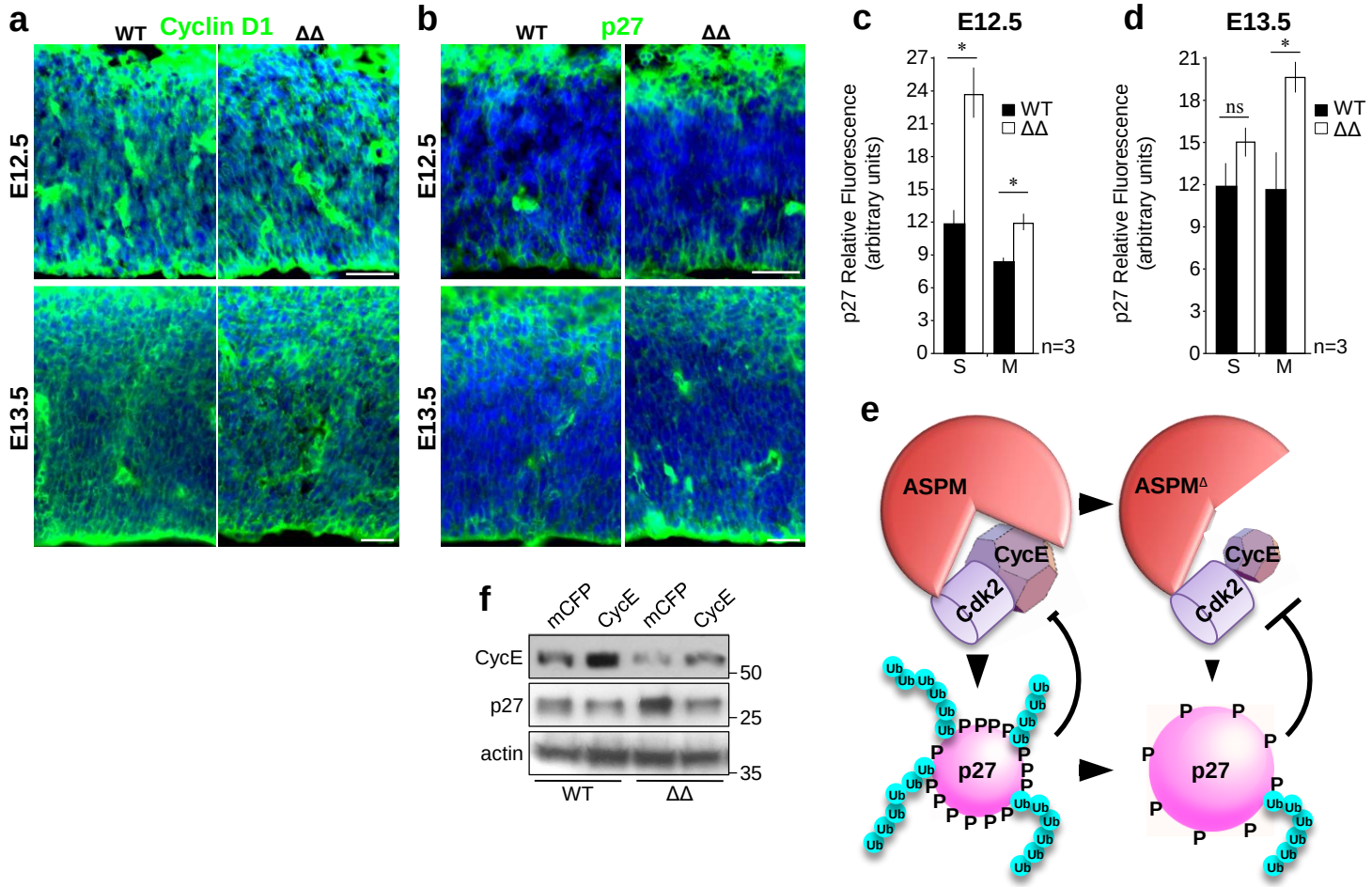

Supplementary Figure 10. Cyclin D1 and p27 expression in early VZ.

(a) Matching E12.5 and E13.5 coronal somatosensory cortical sections of *ASPM*$^{\Delta}$ and their WT littermates stained for Cyclin D1. Similar Cyclin D1 expression pattern between WT and *ASPM*$^{\Delta}$ VZ corresponds to the identical Cyclin D1 protein levels (Fig. 3a) and the equal Cyclin D1 kinase activities (Fig. 3c). Essentially, WT and *ASPM*$^{\Delta}$ VZ exhibited cytoplasmic Cyclin D1 immunoreactivity throughout the entire VZ, with increased levels in M- and S-phase NPC and vasculature structures.

(b) Matching E12.5 and E13.5 coronal somatosensory cortical sections stained for p27 demonstrating similar expression pattern between WT and *ASPM*$^{\Delta}$ VZ. Essentially, WT and *ASPM*$^{\Delta}$ VZ exhibited cytoplasmic p27 immunoreactivity exclusively in M- and S-phase NPC, and in vasculature structures. However, p27 expression appears much stronger in the mutant VZ.

(c-d) Corresponding to the increased p27 protein levels detected by Western blotting (Fig. 3a), cortical *ASPM*$^{\Delta}$ M-phase NPC displayed increased p27 immunofluorescence intensity. E12.5 S-phase NPC also display increased p27 immunofluorescence intensity. * $P < 0.05$, by Student's *t* test. Scale bars represent 50 μm

The Cyclin-dependent Kinase Inhibitor (CKI), p27 plays an important role in regulating the development of neuronal tissues[26-29]. In particular, it has been shown to play an essential role in the development of the cerebral cortex by adjusting NPC internal regulatory mechanisms of proliferation/differentiation behavior and the birth date of cortical neurons[30]. Accordingly, in p27 null mice there is a decrease in neuronal production during mid-corticogenesis and an increase in production of late-born neurons, resulting in an enlargement of upper cortical layers[30, 31]. Conversely, overexpression of p27 in cortical NPC results in a reduction in number of superficial layer neurons[22, 31]. Thus, p27 expression levels in cortical progenitors appear to determine the probability of cell cycle re-entry[32], and differences in p27 expression levels between areas of the developing primate cortex have been implicated in area-specific levels of neuronal production[24]. Although, p27 is a well-established modulator of the G1- to S-phase transition[33], cortical NPC cell-cycle kinetic parameters are not altered even by extreme disregulation of p27 expression, whether the disregulation is either up or down. T_C and T_{G1} are unchanged in VZ–NPC of the p27 null mouse[30], or p27 overexpressing mouse[22]. However, p27 does play a key role in the probability of NPC cell-cycle exit (Q) independently of cell cycle progression[22, 30]. It has been shown to promote neuronal differentiation by stabilizing the Neurogenin2 protein[34]. Therefore, the increase in p27 expression in *ASPM*$^{\Delta}$ NPC could also be accounted for the observed orientation independent premature neuronal differentiation (Fig. 1g,h, 1j). This would also be consistent with the rescue by both Cyclin E lentiviral infection (Fig. 6b) and the blocking of ubiquitination (Fig. 7g).

(e) Although extracts from E12.5 *ASPM*$^{\Delta}$ telencephalon showed enhanced levels of p27 (Fig. 3a), it did not co-IPed with ASPM (Fig. 8b). A working model suggests that via a negative feedback loop, *ASPM*$^{\Delta}$ depleted Cyclin E results in a decreased p27 phosphorylation, reducing its susceptibility to ubiquitination and degradation[35], bringing about increased p27 in *ASPM*$^{\Delta}$.
(f) Cortices of E14.5 embryos were transduced with lentiviral Cyclin E or mCFP control (Fig. 5a). Expression of p27 was determined 48 h later by Western blotting. Essentially, p27 protein levels in Cyclin-E overexpressing *ASPM*$^{\Delta}$ cortices were cut back to WT levels.

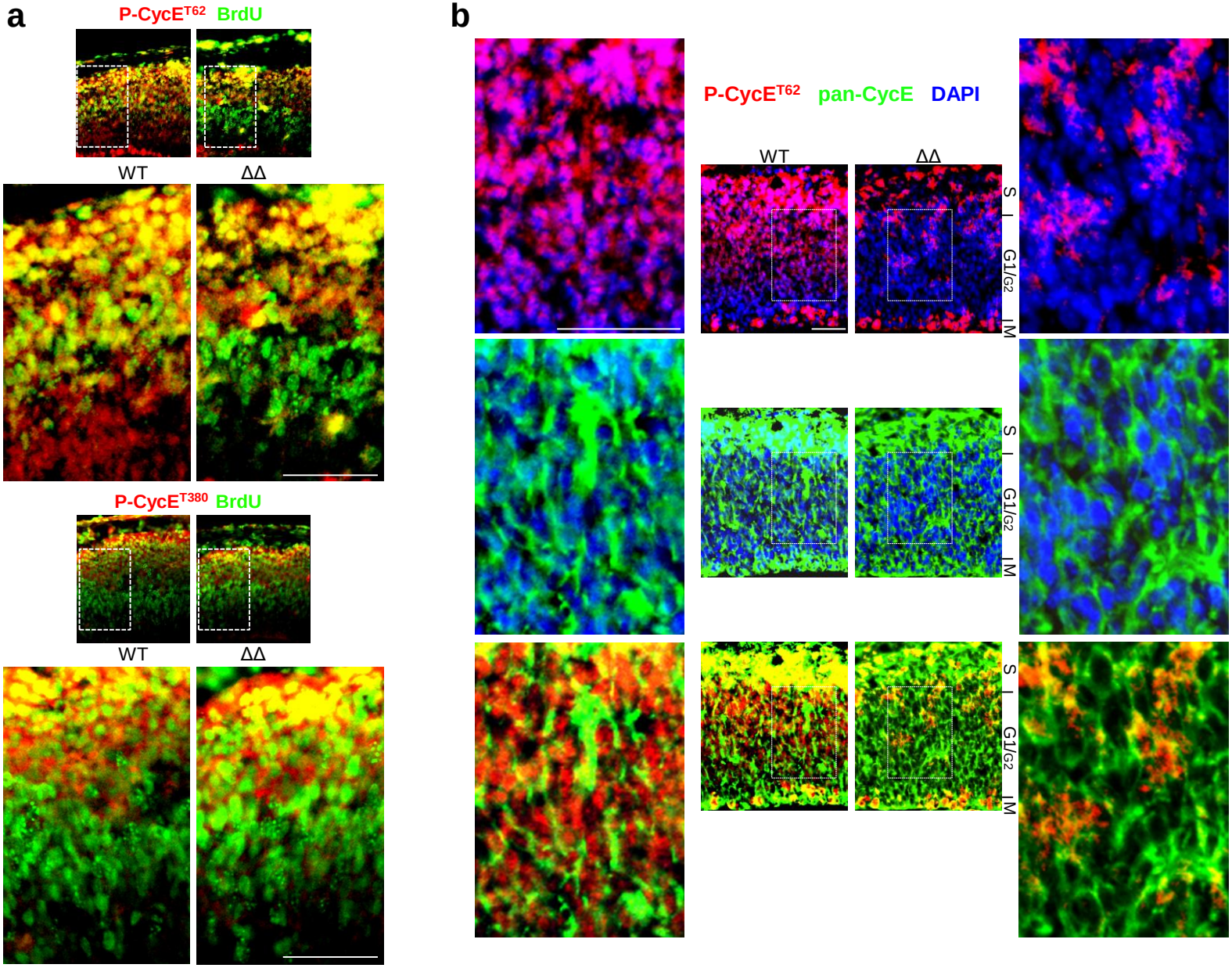

Supplementary Figure 11.

(a) E12.5 coronal cortical sections stained for P-Cyclin E^{T62}, P-Cyclin E^{T380}, and BrdU (30' pulse). High-resolution images of Figure 3d.

(b) E12.5 coronal cortical sections stained for total pan-Cyclin E and P-Cyclin E^{T62}. High-resolution images of Figure 3i.

Scale bars, 50 μm.

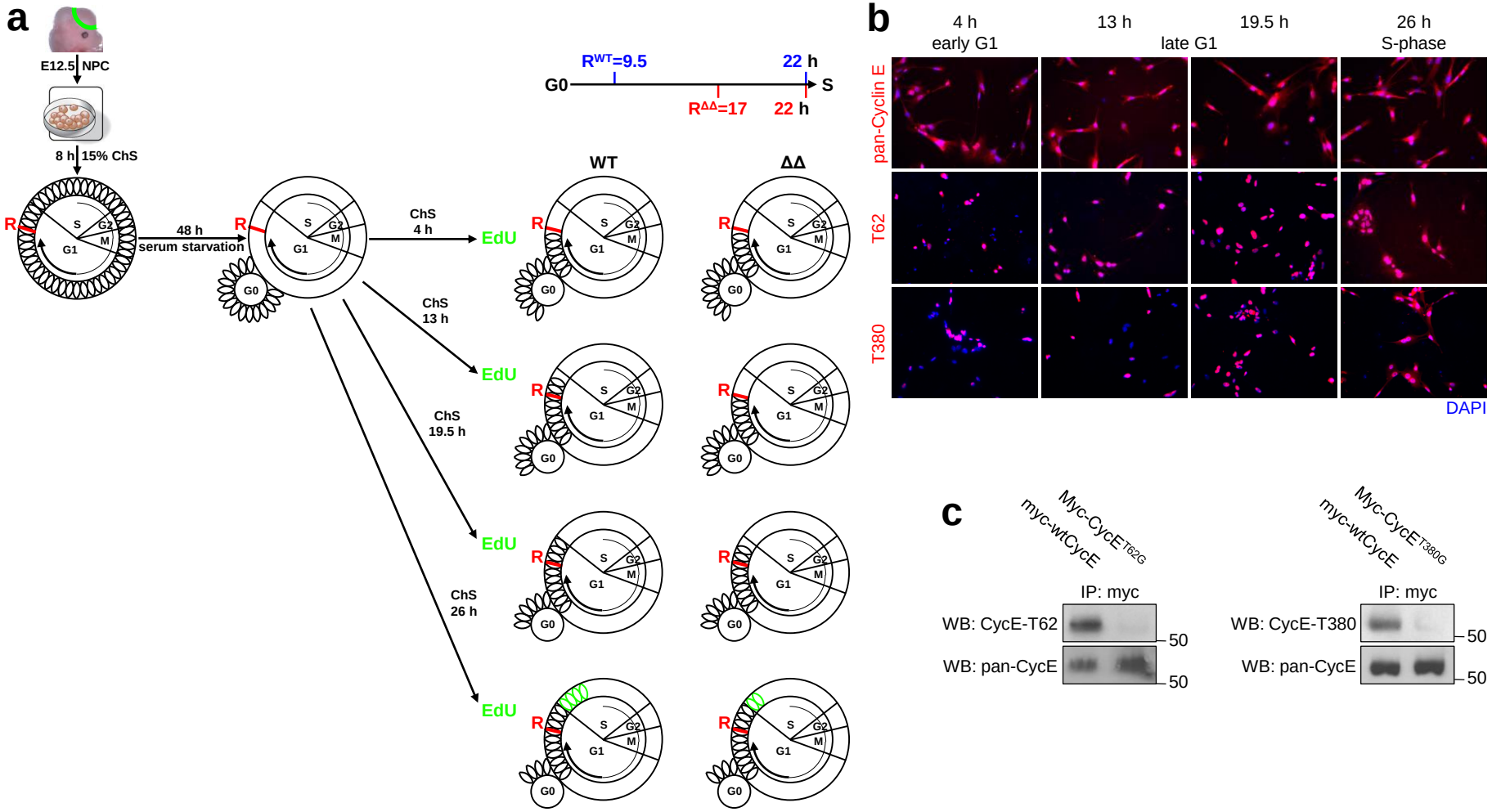

Supplementary Figure 12. Experimental design principles for *in vitro* tracking of Cyclin E expression and phosphorylation along the G_0 to S interval.

(a) E12.5 telencephalic NPC were isolated and allowed to attach for 8 h in neurospheres medium containing 15% chicken serum (ChS) and bFGF. Subsequently, cells were synchronized in G_0 by serum starvation for 48 h in medium containing 0.25% ChS. To initiate cell cycle entry, 15% ChS-supplemented medium was re-applied. EdU tracer was added to the medium at successive time points. After 20 minutes incubation, cells were processed using the Click-iT EdU imaging kit, stained for the indicated antibodies and counterstained with DAPI. Proportions of P-Cyclin E positive NPC (relative to total DAPI-stained nuclei) were plotted against time of ChS stimulation (Fig. 3j,l). In addition, proportions of P-Cyclin E positive/negative NPC relative to EdU labeled nuclei were plotted against time of ChS stimulation (Fig. 3m).

According to the R-point assessment experiments (Fig. 2g,h), an average NPC was still in early G1-phase 4 h past G_0. After 13 h, only WT NPC have past the R-point while *ASPM*$^{\Delta}$ cells were still in early G1. By 19.5 h, also *ASPM*$^{\Delta}$ NPC have reached late G1-phase. Finally, at 26 h all NPC have entered S-phase. (n = 3 independent experiments, > 250 cells per experiment).

(b) Representative fields showing P-Cyclin E^{+} WT-NPC. The IHC, conducted on *in vitro* cultured cells using rabbit anti pan-Cyclin E antibodies, presents a strong support to the *in vivo* observation demonstrated in Figure 3i using different antibodies (mouse anti pan-Cyclin E). In essence, non-phosphorylated Cyclin E showed nuclear and cytoplasmic localization from early G1- all the way to S-phase. Phosphorylated Cyclin E, on the other hand, were mostly nuclear during G1-phase, and acquired further cytoplasmic localization upon reaching S-phase.

(c) myc-tagged wt-Cyclin E, Cyclin E^{T62G}, and Cyclin E^{T380G} were immunoprecipitated from transiently transfected HEK293T cells. The affinity purified myc-tagged proteins were blotted with antibodies directed at pan-, phospho-Thr^{62}, and phospho-Thr^{380} of Cyclin E. Selective interaction with wild-type but not mutated Cyclin E confirms the antibodies specific interactions.

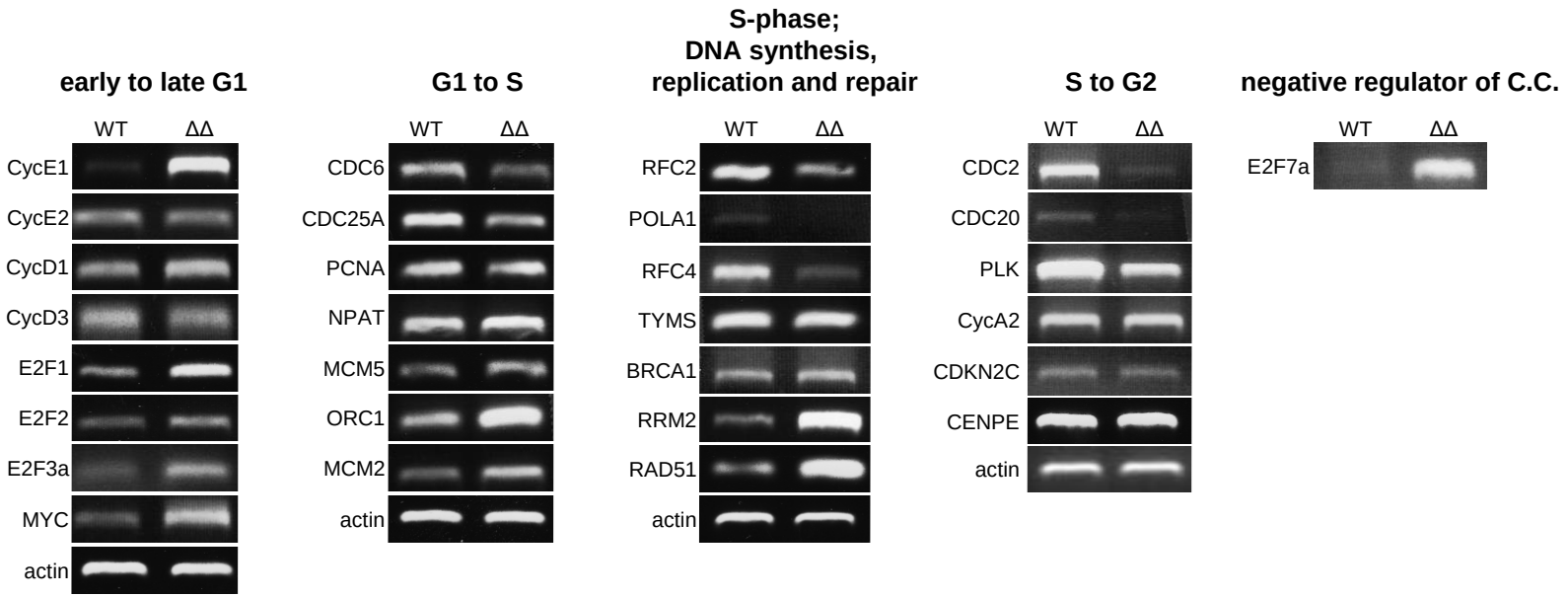

Supplementary Figure 13. Semiquantitative RT-PCR for comparison of expression of E2F targets between *ASPM*$^{\Delta}$ and WT E12.5 NPC. Tabulated by[36] are genes that involve in C.C. progression, DNA synthesis and replication. Note that most genes regulating early to late G1-phase transition are induced in *ASPM*$^{\Delta}$ NPC, suggesting that the cells sense and try to overcome the setback. Additionally, expression of *E2F7*, a family member mediating negative regulation of C.C., is greatly induced, presenting a probable mechanism for the reduced overall E2F activity detected in Figure 4e and inefficient transitions throughout all C.C. phases.

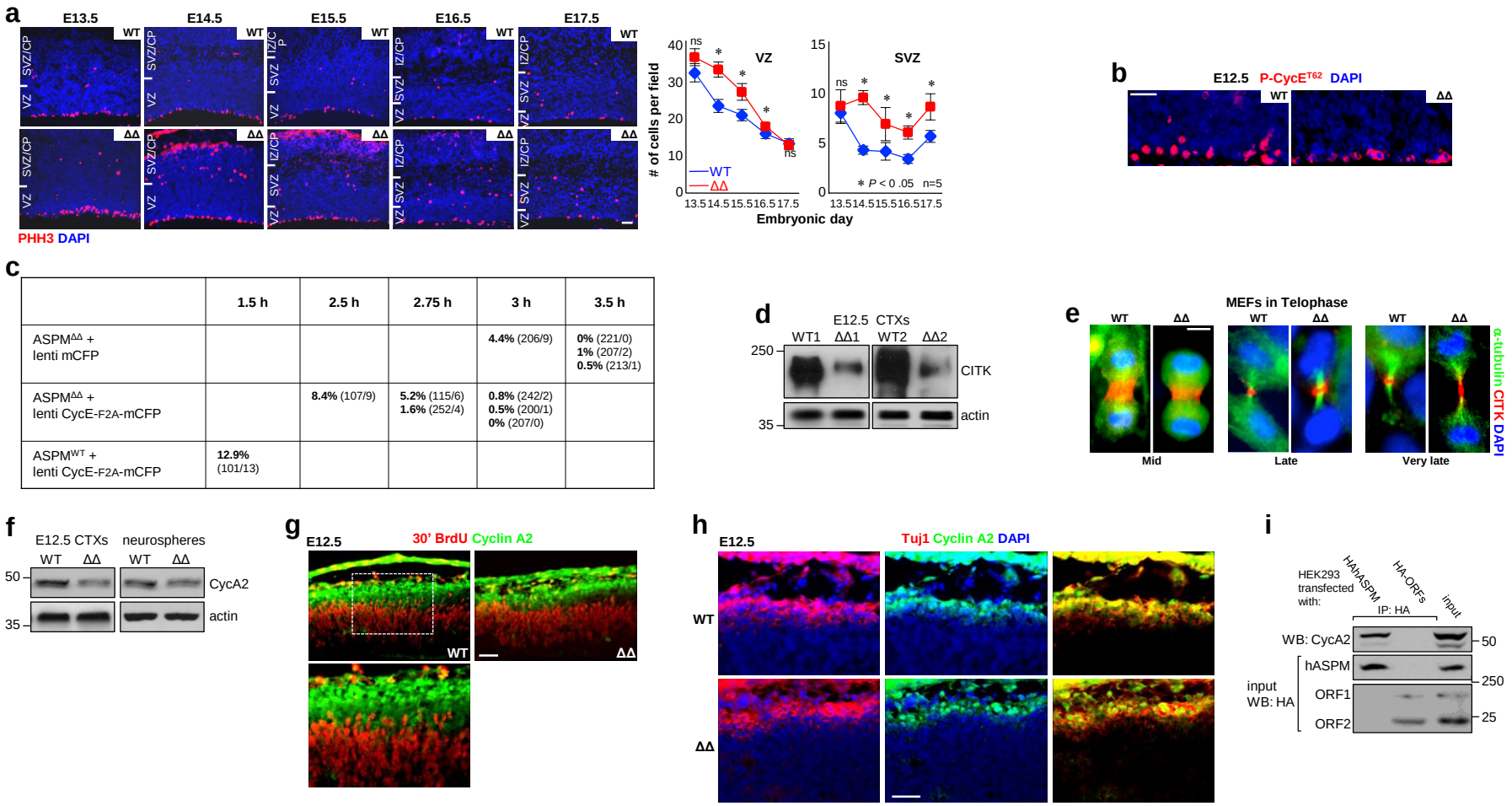

	1.5 h	2.5 h	2.75 h	3 h	3.5 h
ASPM$^{\Delta\Delta}$ + lenti mCFP				**4.4%** (206/9)	**0%** (221/0) **1%** (207/2) **0.5%** (213/1)
ASPM$^{\Delta\Delta}$ + lenti CycE-F2A-mCFP		**8.4%** (107/9)	**5.2%** (115/6) **1.6%** (252/4)	**0.8%** (242/2) **0.5%** (200/1) **0%** (207/0)	
ASPM^{WT} + lenti CycE-F2A-mCFP	**12.9%** (101/13)				

Supplementary Figure 14. Cyclin E dependent and independent ASPM regulation of mitotic succession.
(a) Matching coronal somatosensory cortical sections stained for PHH3 demonstrated over-accumulation of mitotic cells in the VZ (at the ventricular lumen surface) and SVZ (abventricular mitoses) of the *ASPM*$^{\Delta}$ cortex. Increased non-apical PHH3^{+} cells might be attributed to the elongated *ASPM*$^{\Delta}$ SVZ G2/M duration (Supplementary Table 4). Otherwise, the extra SVZ PHH3^{+} cells might result from the change in plane of apical cell division (Fig. 1i) with increased tendency to detach from the VZ region and become SVZ intermediate NPC. Likewise, the increased non-apical PHH3^{+} cells might correspond to the delocalized abventricular Pax6^{+} cells in the *ASPM*$^{\Delta}$ SVZ and IZ (Fig. 1g) that remain proliferative and do not prematurely exit the cell cycle and differentiate. Data are represented as mean ± s.e.m.

(b) Matching E12.5 coronal somatosensory cortical sections stained with anti-P-Cyclin E^{T62} antibodies demonstrated significantly reduced levels of Cyclin E phosphorylated on residue T62 in *ASPM*$^{\Delta}$ mitoses, suggesting a correlation between ASPM and M-phase duration.
(c) Summary of PLM analyses of E15.5 VZ mitoses at increasing survival intervals after pulse labeling with IdU, 24 h after *in utero* lentiviral transductions (see Methods). *In utero* lentiviral transduction rescue just a fraction (one third) of the elongated *ASPM*$^{\Delta}$ M-phase, calling for an additional mechanism of ASPM regulation of M-phase duration in a Cyclin E independent manner.
(d) Protein lysates of E12.5 telencephalic NPC show diminished endogenous citron kinase (CITK) levels in *ASPM*$^{\Delta}$ by Western blotting.
(e) Mid-, late- and very late- telophase MEFs stained for α-tubulin and CITK show delayed progression of ring assembly and furrow ingression. *ASPM*$^{\Delta}$ MEFs in very late telophase exhibit extended intercellular bridge, just as in CITK mutated *Drosophila* neuroblasts[37]. Furthermore, furrow contraction in late telophase was also delayed. CITK is an ASPM interacting partner in mitotic midbody ring[38], therefore proposes an additional mode of regulating M-phase duration. Since Cyclin E does not localize to the midbody ring nor does it co-IP with CITK (not shown) such regulation is Cyclin E-independent.
Scale bars represent 5 μm (e), 20 μm (a), 50 μm (b).

The aforesaid are two non-exclusive scenarios that propose Cyclin E-dependent and independent ASPM regulation of M-phase duration. In the first scenario, ASPM co-localizes with Cyclin E to the centrosomes where it plays an essential role in mitosis termination, G1 progression and S-phase initiation[39-42]. Most of the attention in the literature follows the role played by the Cyclin E/Cdk2 complex in S phase entry due to sharp peak of Cyclin E levels during the late G1 to S phase transition. However, others[43, 44] and we (Fig. 3d, 3l and Supplementary Figure 14b) observed high cytoplasmic and nuclear levels of Cyclin E, mostly phosphorylated, in mitotic cells as well. This suggests that ASPM/Cyclin E play a part in mitosis progression. Indeed, overexpression of ASPM has been shown to relieve the G2/M block imposed by Hepatitis C viral nonstructural protein 5A (NS5A) expression in mouse hepatocytes[45]. Moreover, it took 1.5 hours longer for *ASPM*$^{\Delta}$ NPC to proceed through G2/M phases (Supplementary Tables 3-4). Lentiviral transduced Cyclin E shortened the delay by half an hour (Supplementary Figure 14c). These results correlate with published data demonstrating that aberrant expression of Cyclin E1 or its low molecular weight isoforms inhibited progression through mitosis due to Cyclin E1-Cdh1 binding, which resulted in inhibition of the APC complex and prolonged metaphase[46, 47]. In addition, Cyclin E/Cdk2 phosphorylates Cdc25C. Thus, overexpression of full-length Cyclin E led to premature activation of Cdc25C and prolonged G2/M transition due to arrest in prometaphase[42]. Overexpression of low molecular weight Cyclin E isoforms, on the other hand, led to premature inactivation of Cdc25C and faster mitotic exit[48]. Dysregulation of Cyclin E periodic expression led to mitotic delay associated with genomic instability, chromosome aberrations due to missegregation during metaphase, aberrant anaphase bridges, micronuclei and induction of multipolar anaphases leading to anaphase catastrophe [42, 47, 49].
Similar to *ASPM*$^{\Delta}$ (Supplementary Figure 14a), deletion of the microcephaly disease gene *Wdr62*, resulted in a significant increased number of cortical $PHH3^{+}$ cells associated with mitotic arrest[50]. Like *Wdr62* null mitoses, reduced ASPM protein has been shown to severely perturb a number of aspects of mitosis, including spindle assembly defects and failure to complete cytokinesis[51]. However, unlike *Wdr62* null mice, *ASPM*$^{\Delta}$ mitotic arrest was not associated with increased cell death (Supplementary Figure 1k), induced 4N DNA context, or expended sub-G0 population (Supplementary Figure 7b,c).

The relationship between M-phase duration and mode of mitotic division has been established before[52]. Cells, advancing quickly through mitosis while exhibiting little or no spindle rotation, practice vertical cleavage division. Prolonged mitoses, on the other hand, exhibit extensive spindle oscillation resulting in diagonal or horizontal cleavage planes. ASPM, as part of the microtubule organization center (MTOC) [51, 53, 54], was shown to play an important role in directing the mitotic spindle orientation. The polarization of mitotic cells in response to contacts with the extracellular matrix and neighboring cells results in a *rapid* alignment of the cellular subcortical structure. However, the subcortical polarization signal is *slowly* transmitted to the mitotic spindle through asymmetrically distributed subcortical cues mediated by protein interactions[55]. ASPM interactions with calmodulin and dynein in the spindle poles are essential for Lin-5 localization to the spindle and interaction with the subcortical Lin-5/Gpr-1/2/Ga complex[56]. Hence, ASPM's role in transmitting extracellular signals in order to orient the mitotic spindle and subsequent M-phase duration is clearly Cyclin E-independent. In addition, markedly declining levels of CITK offers another Cyclin E-independent scenario of ASPM-regulated M-phase duration, as progression of ring assembly and mitotic furrow ingression are delayed in late and very late *ASPM*$^{\Delta}$ MEFs in telophase.

(f) Protein lysates of *ASPM*$^{\Delta}$ and WT E12.5 telencephalons, and primary neurospheres were analyzed for endogenous Cyclin A2 protein levels by Western blotting, demonstrating reduced Cyclin A2 in *ASPM*$^{\Delta}$ NPC.
(g) Embryos were pulse labeled for 30 minutes by intraperitoneal BrdU injections to pregnant females. Matching E12.5 coronal somatosensory cortical sections were stained with anti- BrdU and Cyclin A2 antibodies. Although Western blot analysis of E12.5 telencephalic *ASPM*$^{\Delta}$ protein lysates exhibited reduced endogenous Cyclin A2 protein levels, IHC analysis did not reveal significant differences in proportions of NPC expressing Cyclin A2. Importantly, Cyclin A2 expressing cells were not labeled by BrdU, thus are not S-phase cells. Moreover, Cyclin A2 positive cells were located outside of the cycling population of NPC in the superficial primordial plexiform layer composed mainly by subplate and Cajal-Rezius cells.
(h) Matching E12.5 coronal somatosensory cortical sections stained with anti- Tuj1 and Cyclin A2 antibodies. All Cyclin A2 positive cells were also positive for Tuj1, expressed exclusively in differentiated neurons, further supporting the conclusion that Cyclin A2 is not expressed in cycling VZ-NPC.
(i) Corresponding to ASPM co-immunoprecipitation with the Cyclin E/Cdk2 complex (Fig. 8b,c), ASPM also co-immunoprecipitates with Cyclin A2. However, unlike the high molecular weight ubiquitinated smear detected by anti-Cyclin E antibodies in *ASPM*$^{\Delta}$ neurospheres treated with the proteasome inhibitor MG132 (Fig. 7a), no smear was detected by anti-Cyclin A2 antibodies (not shown). Hence, Cyclin A2 is not hyper-ubiquitinated in mutant neurospheres.
Since there is no reliable procedure to precisely measure G2-phase duration in the mouse embryo or to differentiate G2 cell by FACS, we had to broaden the interpretation into *ASPM*$^{\Delta}$ elongated G2/M duration. There is no data available in the literature regarding Cyclin E regulation of G2 progression, suggesting that the elongated G2/M duration is mostly attributed to inhibited mitosis progression. Although, E12.5 *ASPM*$^{\Delta}$ telencephalons exhibited reduced Cyclin A2 (Supplementary Figure 14f), it cannot justify an inhibited G2 progression hypothesis, since Cyclin A2 is exclusively expressed in differentiated neurons but not NPC (Supplementary Figure 12g,h).
Scale bars represent 50 μm.

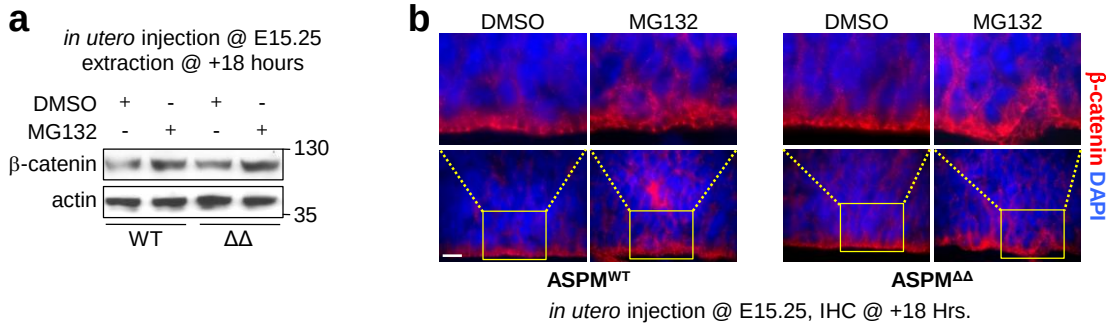

Supplementary Figure 15. Expression of β-catenin in *ASPM*$^{\Delta}$ VZ.
(a) Protein lysates of E16 telencephlones 18 h after *in utero* MG132 administration show increased levels of endogenous β-catenin by Western blotting.
(b) Matching coronal somatosensory cortical sections 18 h after *in utero* MG132 administration show enhanced levels of β-catenin by IHC. Scale bar represents 10 μm.

Overexpression of ubiquitination-resistant β-catenin isoform was shown to override ASPM deficiency[57]. Keeping in mind that MG132 is a ubiquitous proteasome inhibitor that prevents degradation of numerous proteins, the MG132 induced levels of β-catenin offer Cyclin E- and ASPM-independent mechanism of rescuing the unusual excessive *ASPM*$^{\Delta}$ NPC C.C. exit. Transgenic mice expressing the stabilized β-catenin in NPC, developed enlarged brains with folded cortex resembling sulci and gyri, due to expansion of the progenitor pool as a result of reduced NPC differentiation[58]. β-catenin, an integral component of adherens junctions, was proposed to drive more apicobasal divisions. Likewise, though not fully rescuing the irregular *ASPM*$^{\Delta}$ mitotic cleavage orientation, *in utero* administration of MG132 corrected the angle orientation such that it was no longer statistically different from WT (Fig. 7h). Hence, brief *in utero* inhibition of the proteolytic machinery resulting in increased levels of Cyclin E (Fig. 7b,c) and β-catenin, was sufficient to rescue both *ASPM*$^{\Delta}$ related deficiencies (Cyclin E-dependent C.C. progression and β-catenin-dependent mitotic cleavage orientation). Consequently, aberrant *ASPM*$^{\Delta}$ C.C. reentry was perfectly resolved (Fig. 7g).

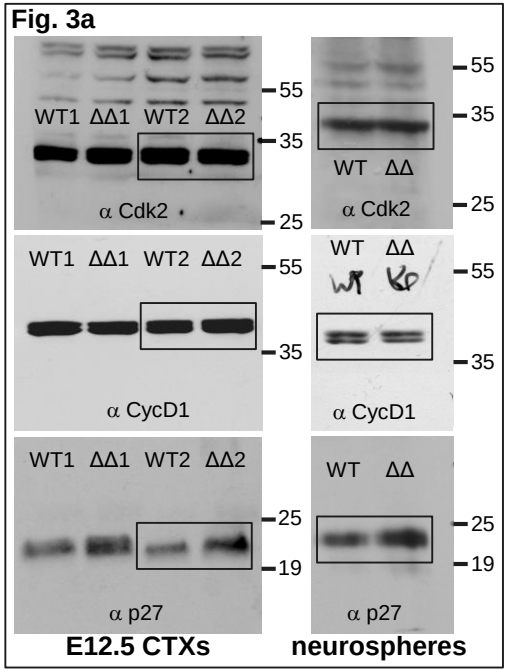

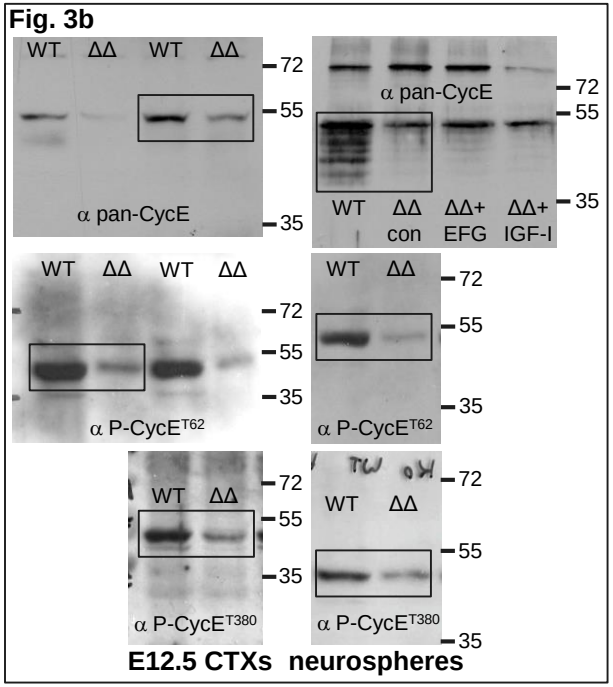

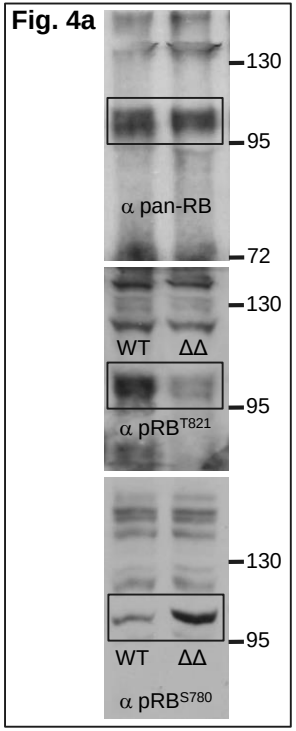

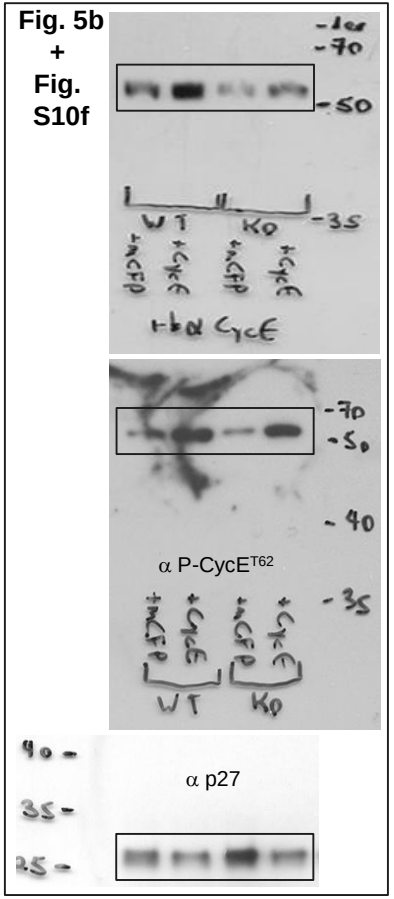

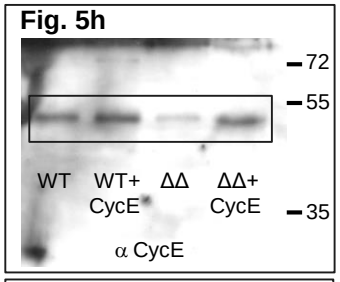

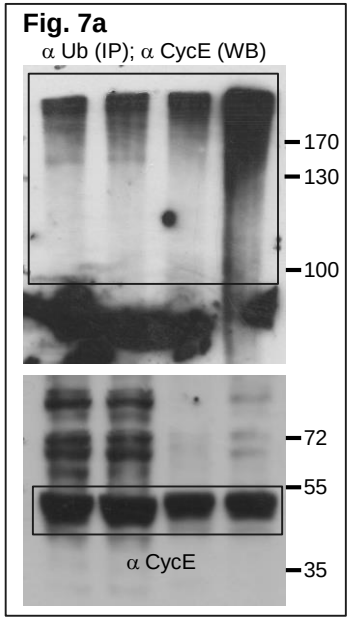

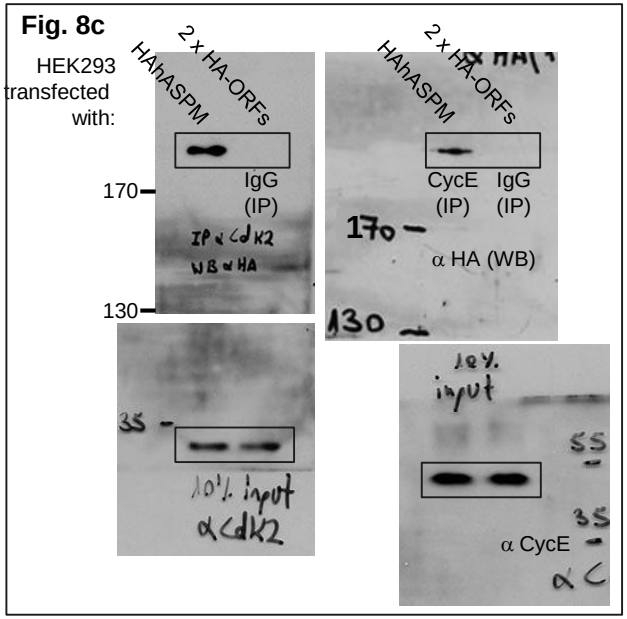

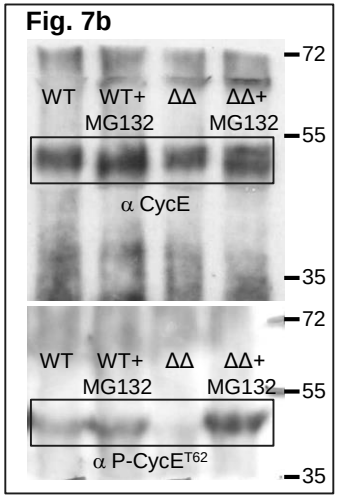

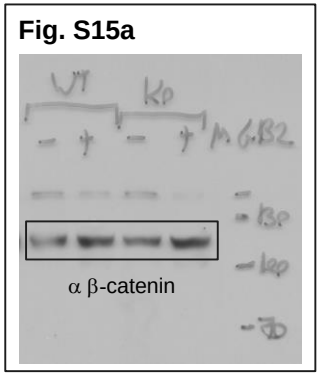

Supplementary Figure 16 Uncropped image blots

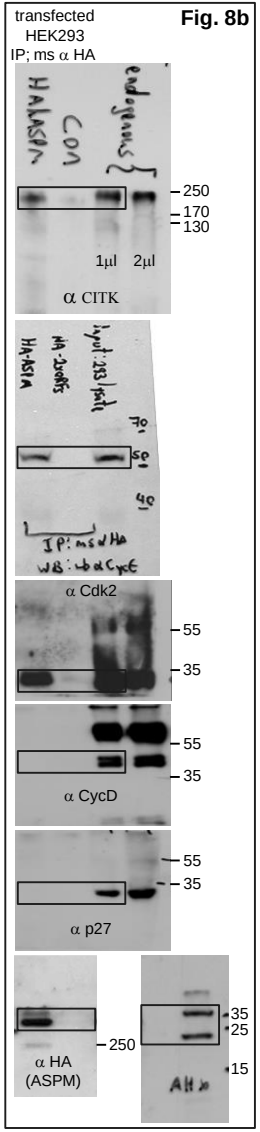

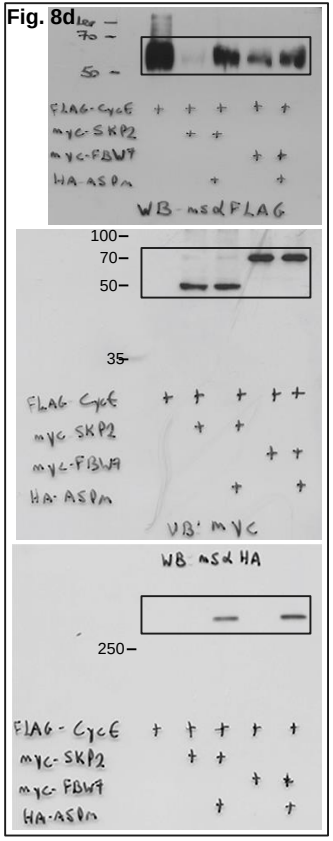

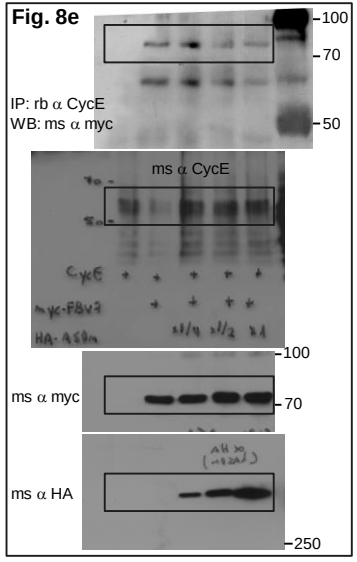

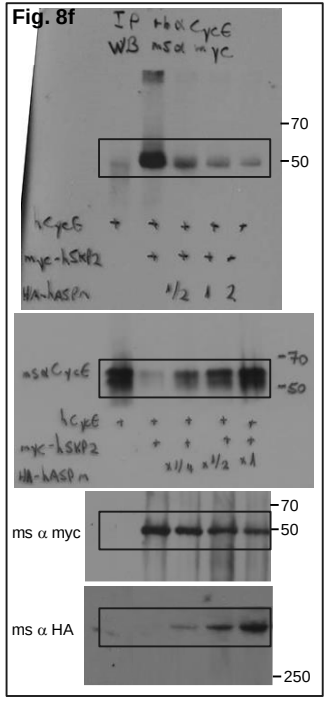

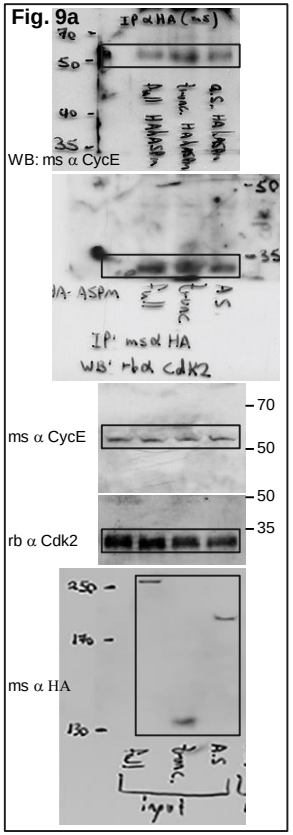

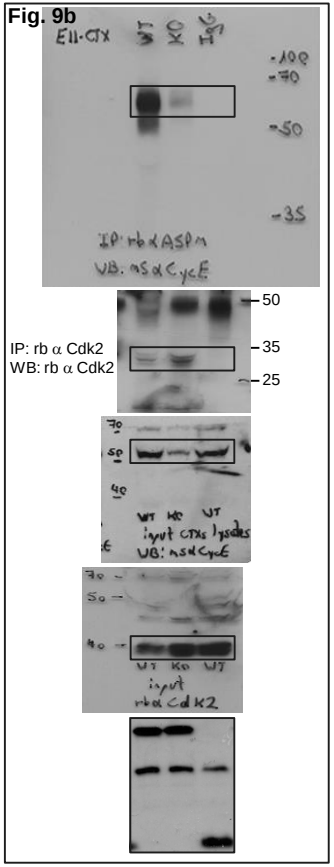

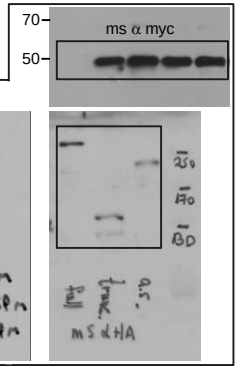

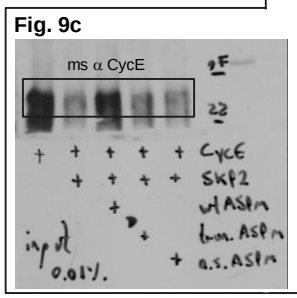

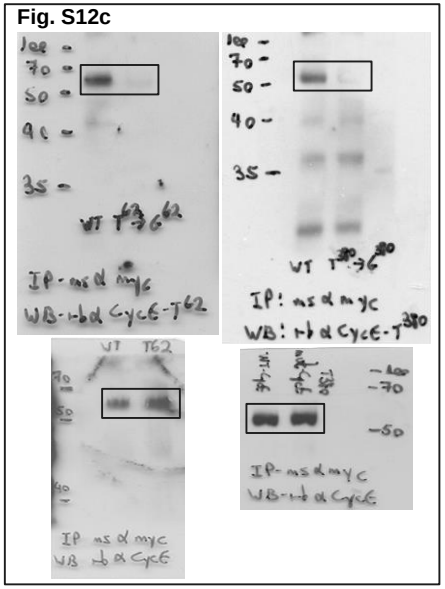

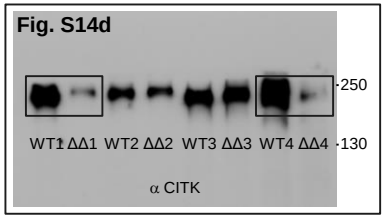

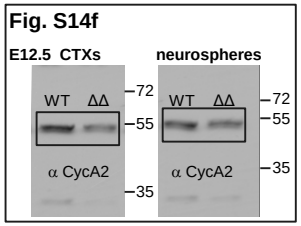

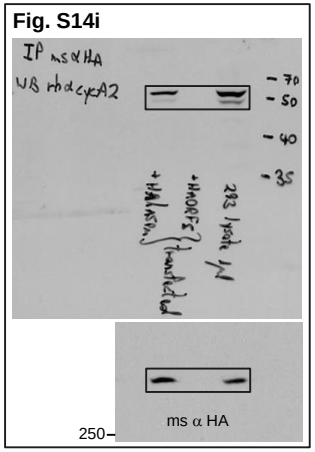

Supplementary Figure 17.
Uncropped image blots

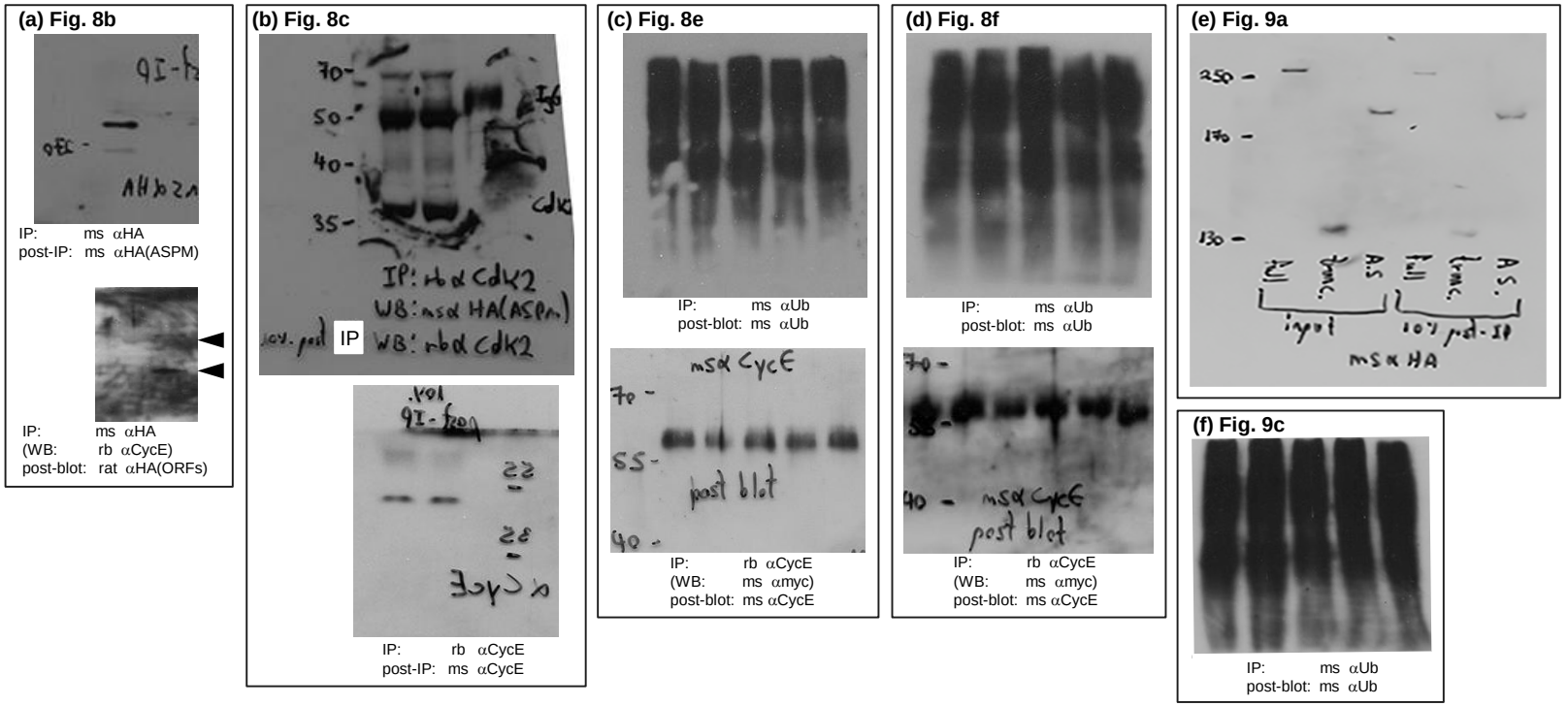

Supplementary Figure 18. Post blots and post-IPs.

(a) Figure 8b, the considerable size differences between ASPM (~410Kd) and the rest of the tested proteins (27-47Kd) posed a problem to generate post-blots. It takes a long run (>36 hours) for the HA-ASPM to enter the gel. Therefore, shorter runs to detect the co-immunoprecipitated proteins are not sufficient. Instead, in order to show the amount of bait proteins that were pull-downed, prior to loading the gel for western blotting, 10% of immunoprecipitants were put aside. These samples were assessed for the amounts of pull-downed HA-ASPM protein after long run, and were termed 10% post-IP. In addition, the co-IP membrane was stripped and immunoblotted with rat anti HA antibodies to produce a post-blot of the HA-tagged ORFs.

(b) Figure 8c, for the same reason as described above, 10% post-IPs are shown instead of post-blots.

(c-d) Figure 8e and 8f, the membranes were stripped and immunoblotted with mouse anti Cyclin E or anti Ub antibodies to produce post-blots.

(e) Figure 9a, for the same reason as described above, 10% post-IP is shown instead of a post-blot.

(f) Figure 9c, the membrane was stripped and immunoblotted with mouse anti Ub antibodies to produce a post-blot.

Age		Genotype	NI	NB	NT	N0
E14.5	**MCZ**	**WT**	43.0 ±4.2	119.3 ±13.0	428.0 ±32.0	266.2 ±45.5
		KO	32.5 ±3.0	116.3 ±12.9	396.2 ±28.2	251.5 ±35.7
	LCZ	**WT**	41.0 ±3.6	123.1 ±10.8	410.1 ±22.1	248.1 ±26.2
		KO	29.8 ±5.4	120.4 ±17.5	386.6 ±20.3	236.7 ±21.7
E15.5	**MCZ**	**WT**	37.0 ±1.9	102.0 ±5.4	422.6 ±15.5	295.8 ±25.5
		KO	29.9 ±3.6	101.7 ±19.6	385.3 ±16.4	263.1 ±22.0
	LCZ	**WT**	32.4 ±3.0	111.6 ±8.5	408.5 ±5.1	274.6 ±15.4
		KO	26.7 ±3.6	107.6 ±13.7	355.5 ±11.9	230.7 ±24.3
E16.5	**MCZ**	**WT**	21.4 ±1.2	70.3 ±8.3	297.2 ±9.8	204.6 ±17.4
		KO	13.1 ±0.7	66.4 ±14.5	272.0 ±2.3	192.4 ±16.4
	LCZ	**WT**	20.3 ±0.9	64.5 ±10.1	338.8 ±3.9	254.1 ±10.2
		KO	13.9 ±1.8	60.4 ±16.6	320.3 ±1.8	245.9 ±18.0

Supplementary Table 1

Mean of cell number in a fixed embryonic cortical area of 500 μm in its medial-lateral dimension and 6 μm (corresponding to section thickness) in its rostral-caudal dimension ± s.e.m.

Values are of NI (IdU-labeled only), NB (BrdU only- plus IdU/BrdU-co-labeled) and NT (all cells) per sector of the VZ in the indicated embryonic day. The *ASPM*$^{\Delta}$ and WT embryos were treated according to the double S-phase labeling protocol (see Supplementary Figure 5). The number of unlabeled cells, N0, was calculated by equation i (Supplementary Figure 5). The values are shown separately for two positions along the medial-lateral axis of the VZ, namely in the medial and lateral cortical zones (MCZ and LCZ, respectively). Cell counts in each brain were performed on six non-adjacent coronal sections to avoid counting the same cell more than once. The analysis was performed on data collected from brains of four embryos for each age and group, one or two mice from each of two or three different litters.

Age		Genotype	T_C (h)	T_S (h)	T_{G2+M} (h)	T_{G1} (h)
E14.5	**MCZ**	**WT**	14.1 ±1.0	5.8 ±0.9	2	6.3 ±1.1
		ΔΔ	17.7 ±1.5 *	7.3 ±0.8*	3.5	6.9 ±1.4
	LCZ	**WT**	14.5 ±1.0	6.2 ±0.7	2	6.3 ±0.9
		ΔΔ	20.1 ±3.1*	8.8 ±1.2*	3.5	7.8 ±2.2
E15.5	**MCZ**	**WT**	17.7 ±2.4	5.5 ±0.3	2	10.2 ±2.3
		ΔΔ	21.4 ±3.4*	7.2 ±0.7*	3.5	10.7 ±3.1
	LCZ	**WT**	18.4 ±1.2	6.6 ±0.4	2	9.8 ±1.2
		ΔΔ	22.0 ±2.3*	8.1 ±0.9*	3.5	10.4 ±2.3
E16.5	**MCZ**	**WT**	20.1 ±0.8	6.6 ±0.5	2	11.5 ±0.9
		ΔΔ	27.9 ±1.1*	10.2 ±1.6*	3.5	14.2 ±1.6*
	LCZ	**WT**	22.7 ±1.3	6.3 ±0.6	2	14.4 ±0.5
		ΔΔ	30.8 ±2.6*	8.4 ±1.3*	3.5	18.9 ±1.4*

Supplementary Table 2

Mean ± s.e.m values of cell cycle parameters for VZ-NPC of the MCZ and LCZ in the indicated embryonic day. T_C and T_S, the length of the overall cell cycle and the S-phase were calculated using the S-phase double-labeling protocol (see Methods), based on data from Supplementary Table 1. The combined length of G_2 and M phase (T_{G2-M}) was evaluated using the PLM method (Supplementary Figure 8 and Supplementary Table 3), and duration of G1-phase (T_{G1}) was calculated by equation iiii (Supplementary Figure 5). Student's *t* test was used to calculate statistical significance with $P < 0.05$ representing a statistically significant difference (*).

Age	Survival time		
	2 Hours	3 Hours	3.5 Hours
E14.5	0.5% (200/1)		
	2.0% (247/5)		
	1.0% (202/2)		
	8.5% (107/10)	2.4% (202/5)	0.9% (223/2)
			0% (211/0)
			0.4% (233/1)
E15.5	0.5% (207/1)		
	0.9% (213/2)		
	0% (202/0)		
		6.7% (283/19)	0.3% (312/1)
			1.7% (234/4)
			0% (200/0)
E16.6	0.4% (228/1)		
	0.9% (225/2)		
	0% (208/0)		
	7.0% (133/10)	4.4% (283/13)	0.5% (200/1)
			0.5% (203/1)
			0.9% (331/3)

Supplementary Table 3

Summary of the percentage of labeled mitoses (PLM) (Supplementary Figure 8) analyses for E14.5, El5.5 and El6.5 cortical VZ-NPC of *ASPM*$^{\Delta}$ (red) and WT (blue) embryos at increasing survival intervals after pulse labeling with IdU. For each embryo, the PLM was determined over at least 200 PHH3^{+} mitoses at the base of the ventricular zone. The $T_{G2\text{-}M}$ was determined according to the cut-off value of 98% of labeled mitoses. Three embryos from 2 litters were used to assess $T_{G2\text{-}M} \leq$ (X) hours, and one embryo was sufficient to determine that $T_{G2\text{-}M} >$ (X) hours. The results indicate that in WT cortices $T_{G2\text{-}M}$ lasted 2 h while in *ASPM*$^{\Delta}$ it was 3.5 h, regardless of embryonic stage.

2 Hours	3.5 Hours	4 Hours	4.5 Hours	5 Hours	5.5 Hours	6 Hours
16.7% (32/160)	5.0% (10/191)	3.2% (6/184)	0.5% (1/209)			
			0% (0/206)			
			0.9% (2/213)			
19.8% (23/93)	8.7% (9/94)	6.6% (8/114)	3.2% (6/184)	8.5% (17/183)	2.9% (7/240)	1.6% (5/317)
						1.5% (4/274)
						1.6% (4/241)

Supplementary Table 4

Summary of the percentage of labeled mitoses (PLM) analyses for El6.5 cortical SVZ-NPC of *ASPM*$^{\Delta}$ (red) and WT (blue) embryos as in Supplement Table 3. The results indicated that in WT SVZ-cortices $T_{G2\text{-}M}$ lasted 4.5 h while in *ASPM*$^{\Delta}$ it was 6 h (Fig. 2e).

Supplementary Table 5, Primers used for RT-PCR;

gene	sense	antisense
β-actin	gatgacgatatcgctgcgctg	gtacgaccagaggcatacagg
BRCA1	gcagaaaatcttagagtgtccg	ctgacacggttccggtagcc
CDC2	tttcaagaaggacaaaggtgcc	actgataagttctagctgagcc
CDC6	ggaaaaactgcctgtttaagcc	ttctgtccgtgagatctaggg
CDC20	aaaccagccggaagacaggg	gattcaggtagtagtcattccg
CDC25A	gaccagctggaaggactggg	tcagggctgggctacatccc
CDK2	tgtggcgcttaagaagatccg	cagaagaatttcaggtgctcgg
CDKN2C	gcaaaataatgtaaacgtcaacgc	cccatttgcctccatcaggc
CENPE	tctgtgttcgtgtgcgaccc	cagtcctattggtgtcttccc
Cyclin A2	gcttcagcttgtaggcacgg	ggtatatccagtctgttgtgcc
Cyclin D1	gcatgcacagacctttgtggc	tctgttcctggcaggcacgg
Cyclin D3	gtggctccatggcagttgcgg	aggcagtccacttcagtgcc
Cyclin E1	tgaaagaagaaggtggctccg	tccaaacctcttctctattgcc
Cyclin E2	cttgaagagaatgtcaagacgc	gtgtttcaatgataatgcaaggg
E2F1	attggtaagcggcttgaaggc	ccgtctgcactctcctccg
E2F2	ctttttgtgcgatgtgcaccc	caaatagttccctgcctaccc
E2F3	agagcctacaaatccatttggc	tgctgtaaaaggttggctggg
E2F7	catagaagaaagccaagataccc	ttgcacacactcggatctggc
MCM2	ctctggtggaggagctgcg	cgggactctcctggatgcg
MCM5	ctcatctccaagagcatttccc	tatcactgaggcagtcaagcc
MYC	cttaaaattctgtcacaacagcc	aaatgctgtgttatcctgaccc
NPAT	ccctcggatgtagccaggc	ctctgatgggcagcaaaccc
ORC1	tggaaagtaaacttcttgatggg	tggtcagcacatacaagtggg
PCNA	gacacataccgctgcgaccg	gcatatacgtgcaaattcaccc
PLK	cacagggacctcaagctggg	cactgggttgatgtgcttggg
POLA	cagatccaaacttagagatggg	cttcacttttaccttgtttccc
RAD51	ccgtggtggaggtgaaggg	gagtagtctgttctgtaaaggg
RFC2	gcagtcctggaactcaatgcc	attttgtctgaagcattacacgc
RFC4	aaagtcaaaccagttccttggg	aagggaggacatggcttccc
RRM2	ggctgacaaggagaacacgc	cttgaacttcttggctaaatcgc
TYMS	gcatgcaggcacgatacagcc	gcatcccagattctcactccc

Supplementary Table 6, Antibodies and dilutions

Target	Dilution	Host	Supplier	Catalog #	Label/clone
actin	1:10000 WB	rabbit	Santa Cruz	SC-7210	
α-tubulin	1:1000 IHC	rabbit	Thermo Scientific	AB-9281-PO	
ASPM	1:100 WB 1:50 IP 1:200 IHC	rabbit	Bethyl Labs	IHC-00058	
β-catenin	1:500 IHC 1:1000 WB	rabbit	Epitomics	1247-1	E247
β-III-tubulin (Tuj1)	1:1000 IHC	mouse	Covance	MMS-435P	
BrdU	1:15 IHC	rat	Axyll	OBT0030S	H8425
	1:4 IHC	mouse	DSHB	G3G4	* Developed by Dr. S.J. Kaufman
Brn1	1:2000 IHC	guinea pig			Kindly provided by Dr. M. Wegner
Cdk2	1:200 WB 1:50 IP	rabbit	Santa Cruz	sc-748	H-298
ChdU (BrdU)	1:50 IHC	rat	Novus	Nb500-169	BU1/75(ICR1)
Citron Kinase	1:500 IHC 1:1000 WB	mouse			Kindly provided by Dr. J. LoTurco
Ctip2	1:500 IHC	rat	Abcam	ab18465	25B6
Cux1 (CDP)	1:1000 IHC	rabbit	Santa Cruz	sc-13024	M-222
Cyclin A2	1:500 IHC 1:1000 WB	rabbit	GeneTex	GTX103042	N1C1
Cyclin D1	1:100 WB 1:25 IP	rabbit	Thermo Scientific	RM-2113	
	1:1000 IHC	mouse	Cell Signaling	2926S	DCS6
Cyclin E	1:500 IHC 1:40 WB	mouse	Covance	SIG-3903-1000	
	1:1000 WB 1:200 IP	rabbit	Millipore	07-687	
	1:2000 WB 1:200 IP	rabbit	Santa Cruz	sc-481	M-20
Flag	1:200 WB 1:2000 IP	mouse			**
GFAP	1:250 IHC	mouse	BD Biosciences	556327	4A11
HA	1:200 WB 1:2000 IP	mouse			**
	1:100 WB	rat	Roche	11815016001	3F10
IdU (BrdU)	1:25 IHC	mouse	BD Biosciences	347580	IgG1k
Ki67	1:500 IHC 1:500 FACS	mouse	BD Pharmingen	550609	
myc	1:200 WB 1:2000 IP	mouse			**
p27Kip1	1:500 IHC 1:2000 WB	mouse	BD Biosciences	K25025-050	610243
Pax6	1:300 IHC	rabbit	Covance	PRB-278P	
PCNA	1:200 IHC	Mouse	Millipore (Chemicon)	MAB424R (7-06-0)	PC10 IgG2a
PHH3	1:500 IHC	rabbit	Millipore	05-817R	Ser10
phospho Cyclin E Thr62	1:500 IHC 1:200 WB	rabbit	Cell Signaling	4136S	
phospho Cyclin E Thr380	1:500 IHC 1:200 WB	rabbit	BioSS	bs-3120S	referred to as Thr380 according to[59-61]
pS780 phospho-Rb	1:500 WB	rabbit	Cell Signaling	9307S	
pS821 phospho-Rb	1:250 WB 1:500 IHC	rabbit	Invitrogen (Biosource)	44582G	
Rb	1:40 WB	Mouse	DSHB	4.1-s	* Developed by Dr. J. Sage
RC2	1:4 IHC	Mouse	DSHB		* Developed by Dr. M. Yamamoto
Tbr1	1:1000 IHC	rabbit	Chemicon	AB9616	
Ubiquitin	0.2 mg/ml IP	mouse	Santa Cruz	sc-8017	P4D1
	0.2 mg/ml IP	mouse	Cell Signaling	3936	P4D1

* Obtained from the Developmental Studies Hybridoma Bank developed under the auspices of the NICHD and maintained by the University of Iowa, Department of Biology, Iowa City, IA 52242.

** Obtained from the Bioprocessing Resource, Huntsman Cancer Institute, U of Utah.

For Immunofluorescence appropriate Alexa Fluor dye–conjugated secondary antibodies (1:1000, Invitrogen) were used. Protein bands on immunoblots were visualized with HRP-labeled goat anti-rabbit or anti-mouse IgG followed by detection with chemiluminescence.

Supplementary Note 1. Figure 1g demonstrates displaced abventricular Pax6^{+} foci located in heterotopic positions outside the VZ in E15.5 and E16.5 *ASPM*$^{\Delta}$ cortices (arrowheads). Similar far-basal Pax6^{+} cells located in the SVZ and intermediate zone (IZ) regions that would normally have been occupied by differentiated neurons have been previously described in mutant embryos with abnormally developed cortices[62-65]. This has been shown to result from a premature detachment of VZ radial glial cells from the ventricular surface due to loss of both basal and apical end feet attachments. Nevertheless, the SVZ and IZ Pax6^{+} cells maintained their radial glial molecular phenotype and remained proliferative and undifferentiated, even in the aberrant regions.

Supplementary Note 2. The cartoon depicted in Figure 3k summarizes the interpretation of data shown in Figures 3d-3j. It represents cellular localization of Cyclin E along the inter-nuclear movement of WT VZ-NPC. Because cells between M- and S-phase zones are overwhelming in the G1, G2 cells are not discussed. Cyclin E is mostly not phosphorylated in early G1-phase, therefore resides in the cytoplasm. As cells transverse the R-point into late G1, increasing amount of Cyclin E is being phosphorylated, mainly on residue T62, and translocated to the nucleus while non-phosphorylated Cyclin E remains cytoplasmic. Gradually nuclear Cyclin E is being phosphorylated on residues T380. During S-phase all Cyclin E is phosphorylated and distributed along all cellular compartments. Mitotic cells contain high levels of nuclear and cytoplasmic P-Cyclin E whereas non-phosphorylated Cyclin E retracts to the cytoplasm. Inferred from Figure 8a, Cyclin E mainly concentrates in anaphase spindle poles.

Supplementary Methods

Quantitative fluorescence intensity analysis. All quantifications of fluorescence intensity were performed using ImageJ software according to[66]. Identical acquisition exposure-time parameters were used to capture images. A region was drawn around each cell to be measured. Integrated Density (the sum of the intensity of the pixels for one cell) was determined. A second region without fluorescent objects just beside to the selected cell was drawn to used for background subtraction. The net average fluorescence intensity of a pixel in the region of interest was then calculated with the following formula:
Corrected Total Cell Fluorescence (CTCF) = (Integrated Density) – (Area of selected cell) X (Mean Fluorescence of background readings).
Average of corrected intensity values of 50 cells were calculated per cortex.

Determination of the Q fraction. At each passage through the NPC-C.C., the proportion of daughter cells that exit the C.C. and are no longer proliferating (**Q**uiescence fraction cells) increases from 0 at the onset of the corticogenesis to 1 at the end of the corticogenesis. The proportion of daughter cells that re-enter the C.C. and remain **P**roliferative (P fraction) changes in a complementary trend from 1 at the onset of the corticogenesis to 0 at the end of the corticogenesis[22, 67-71]. BrdU was administered as a single i.p. injection to pregnant dams. Embryos were collected after 24 h and coronal sections were stained for Ki67 and BrdU. This design identifies the cohort of Q-cells that exit the C.C. as those that are positive for BrdU but negative for Ki67. Q fraction cells are presented as the percentage of total BrdU-positive cells.

Cell cycle analysis by FACS. E12.5 telencephalic lobes or E15.5-E16.5 cerebral cortex hemispheres were dissected and digested for 30 minutes at 37^0C with 500 U/ml papain (Worthington) and 100 U/ml DNase I (Fermentas) in PBS with rocking followed by gentle repeated pipetting to dissociate cells. 5 x 10^7 E15.5-E16.5 cells were resuspended in 50 ml ice-cold 75% ethanol while vortexing, and further fixed at -20^0C for 2 h. Subsequent to adequate washings in FACS buffer (0.5% BSA, 0.05% NaN3 in PBS), cells were successively stained with primary anti-Ki67 and the appropriate secondary antibody for 30 minutes at RT in FACS buffer, and post-fixed 15 minutes with 2% PFA. E12.5 freshly isolated cells or Ki67 stained cells were incubated with 0.1% Triton X-100, 0.5 mM EDTA, 0.05 mg/ml RNase A (Qiagen), and 50 μg/ml propidium iodide (Sigma-Aldrich) in PBS at 4^0C for 1-2 h, before analyses. Cells were analyzed with a BD FACScan flow cytometer (BD Biosciences), and cell cycle gating was examined using FLOWJO - Flow Cytometry Analysis Software.

Preparation of lentiviral vectors. A Cyclin E expression vector was constructed by replacing the native IRES-hrGFP in CSII-EF-MCS-IRES-hrGFP lentiviral expression vector[72, 73] with a full-length Cyclin E1 cDNA. The Cyclin E stop codon was removed and the cDNA was linked to a DNA fragment encoding in frame the FMDV 2A sequence[74] and membrane bound mCerulean (mCFP) (addgene). A mCerulean fragment was also inserted instead of the IRES-hrGFP, thus creating a mCFP expression vector that served as control. A transient-transfection system was used to create lentiviruses harboring Cyclin E cDNA. HEK293T cells were transfected by HIV-1-based lentiviral vectors according to[72, 73]. Viruses were subsequently concentrated from conditioned media harvested 48 h after transfection by ultracentrifugation at 25,000 rpm in a Beckman SW28 swinging bucket rotor. The pellet was resuspended in sterile PBS. Viral titers, determined by QuickTiter^{TM} Lentivirus Titer Kit (Cell Biolabs Inc. VPK-107), were on average 5×10^7 to 1×10^8 Lentiviral particles (LP)/ml. For rescue assays, freshly isolated E12.5 or E14.5 NPC were immediately infected with 1 μl of viral suspension in 0.5 or 1 ml media, and cells were seeded and treated as described above for pair-cell or neurospheres analyses, respectively. Adherent cells were cultured for 24 h before fixation. Neurospheres were cultured for 6 days before examination. Expression of the reporter mCFP gene, under control of the EF-1α promoter, confirmed ~40% infection efficiency of neurospheres and >90% for the pair-cell analysis, for both Cyclin E-F2A-mCFP and mCFP vectors.

Cell cultures. HEK293T cells (kindly provided by Dr. Y. Groner, WIS, Rehovot, Israel) were maintained in Dulbeco's modified Eagle's medium (DMEM) supplemented with 10% fetal bovine serum at 37^0C in a humidified incubator containing 7.5% CO_2. Calcium phosphate was used for plasmid transfection as previously described[75].

Coimmunoprecipitation. Lysates of MG132 treated neurospheres (6 h, 20 μM, Sigma-Aldrich) or HEK293T cells transiently expressing HA-tagged respective proteins were incubated overnight at 4^0C with anti-HA or anti-Ub antibodies, respectively, cross-linked (dimethyl pimelimidate) to Dynabeads Protein G (invitrogen). Adequately washed bound material was subsequently eluted by 50 mM Glycine (pH 2.8) and boiled for 10 minutes. The immunoprecipitants and input samples were analyzed by standard Western blotting procedure for ubiquitinated Cyclin E or for endogenous proteins.

Whole mount *in situ* hybridization. Synthesis of the RNA in situ probe was performed according to manufacturer's directions (Roche BioSciences). The hybridization was carried out according to[76].

SUPPLEMENTARY REFERENCES

1. Kaindl, A.M. *et al.* Many roads lead to primary autosomal recessive microcephaly. *Prog Neurobiol* **90**, 363-383 (2010).
2. Nicholas, A.K. *et al.* The molecular landscape of ASPM mutations in primary microcephaly. *J Med Genet* **46**, 249-253 (2009).
3. Wu, S., Ying, G., Wu, Q. & Capecchi, M.R. A protocol for constructing gene targeting vectors: generating knockout mice for the cadherin family and beyond. *Nat Protoc* **3**, 1056-1076 (2008).
4. Bond, J. *et al.* ASPM is a major determinant of cerebral cortical size. *Nat Genet* **32**, 316-320 (2002).
5. Kouprina, N. *et al.* The microcephaly ASPM gene is expressed in proliferating tissues and encodes for a mitotic spindle protein. *Hum Mol Genet* **14**, 2155-2165 (2005).
6. Paik, J.H. *et al.* FoxOs cooperatively regulate diverse pathways governing neural stem cell homeostasis. *Cell Stem Cell* **5**, 540-553 (2009).
7. Takahashi, T., Nowakowski, R.S. & Caviness, V.S., Jr. Cell cycle parameters and patterns of nuclear movement in the neocortical proliferative zone of the fetal mouse. *J Neurosci* **13**, 820-833 (1993).
8. Takahashi, T., Nowakowski, R.S. & Caviness, V.S., Jr. The cell cycle of the pseudostratified ventricular epithelium of the embryonic murine cerebral wall. *J Neurosci* **15**, 6046-6057 (1995).
9. Siegenthaler, J.A. & Miller, M.W. Transforming growth factor beta 1 promotes cell cycle exit through the cyclin-dependent kinase inhibitor p21 in the developing cerebral cortex. *J Neurosci* **25**, 8627-8636 (2005).
10. Yingling, J. *et al.* Neuroepithelial stem cell proliferation requires LIS1 for precise spindle orientation and symmetric division. *Cell* **132**, 474-486 (2008).
11. Calegari, F., Haubensak, W., Haffner, C. & Huttner, W.B. Selective lengthening of the cell cycle in the neurogenic subpopulation of neural progenitor cells during mouse brain development. *J Neurosci* **25**, 6533-6538 (2005).
12. Calegari, F. & Huttner, W.B. An inhibition of cyclin-dependent kinases that lengthens, but does not arrest, neuroepithelial cell cycle induces premature neurogenesis. *J Cell Sci* **116**, 4947-4955 (2003).
13. Lange, C., Huttner, W.B. & Calegari, F. Cdk4/cyclinD1 overexpression in neural stem cells shortens G1, delays neurogenesis, and promotes the generation and expansion of basal progenitors. *Cell Stem Cell* **5**, 320-331 (2009).
14. Pilaz, L.J. *et al.* Forced G1-phase reduction alters mode of division, neuron number, and laminar phenotype in the cerebral cortex. *Proc Natl Acad Sci U S A* **106**, 21924-21929 (2009).
15. Artegiani, B., Lange, C. & Calegari, F. Expansion of embryonic and adult neural stem cells by in utero electroporation or viral stereotaxic injection. *J Vis Exp* (2012).
16. Artegiani, B., Lindemann, D. & Calegari, F. Overexpression of cdk4 and cyclinD1 triggers greater expansion of neural stem cells in the adult mouse brain. *J Exp Med* **208**, 937-948 (2011).
17. Nonaka-Kinoshita, M. *et al.* Regulation of cerebral cortex size and folding by expansion of basal progenitors. *EMBO J* **32**, 1817-1828 (2013).
18. Nieto, M. *et al.* Expression of Cux-1 and Cux-2 in the subventricular zone and upper layers II-IV of the cerebral cortex. *J Comp Neurol* **479**, 168-180 (2004).
19. Cubelos, B. *et al.* Cux1 and Cux2 regulate dendritic branching, spine morphology, and synapses of the upper layer neurons of the cortex. *Neuron* **66**, 523-535 (2010).
20. Hevner, R.F. *et al.* Tbr1 regulates differentiation of the preplate and layer 6. *Neuron* **29**, 353-366 (2001).
21. Hayes, N.L. & Nowakowski, R.S. Exploiting the dynamics of S-phase tracers in developing brain: interkinetic nuclear migration for cells entering versus leaving the S-phase. *Dev Neurosci* **22**, 44-55 (2000).
22. Tarui, T. *et al.* Overexpression of p27 Kip 1, probability of cell cycle exit, and laminar destination of neocortical neurons. *Cereb Cortex* **15**, 1343-1355 (2005).
23. Miyama, S., Takahashi, T., Nowakowski, R.S. & Caviness, V.S., Jr. A gradient in the duration of the G1 phase in the murine neocortical proliferative epithelium. *Cereb Cortex* **7**, 678-689 (1997).
24. Lukaszewicz, A. *et al.* G1 phase regulation, area-specific cell cycle control, and cytoarchitectonics in the primate cortex. *Neuron* **47**, 353-364 (2005).
25. Quastler, H. & Sherman, F.G. Cell population kinetics in the intestinal epithelium of the mouse. *Exp Cell Res* **17**, 420-438 (1959).
26. Fero, M.L. *et al.* A syndrome of multiorgan hyperplasia with features of gigantism, tumorigenesis, and female sterility in p27(Kip1)-deficient mice. *Cell* **85**, 733-744 (1996).
27. Carruthers, S., Mason, J. & Papalopulu, N. Depletion of the cell-cycle inhibitor p27(Xic1) impairs neuronal differentiation and increases the number of ElrC(+) progenitor cells in Xenopus tropicalis. *Mech Dev* **120**, 607-616 (2003).
28. Kiyokawa, H. *et al.* Enhanced growth of mice lacking the cyclin-dependent kinase inhibitor function of p27(Kip1). *Cell* **85**, 721-732 (1996).

29. Delalle, I., Takahashi, T., Nowakowski, R.S., Tsai, L.H. & Caviness, V.S., Jr. Cyclin E-p27 opposition and regulation of the G1 phase of the cell cycle in the murine neocortical PVE: a quantitative analysis of mRNA in situ hybridization. *Cereb Cortex* **9**, 824-832 (1999).
30. Goto, T., Mitsuhashi, T. & Takahashi, T. Altered patterns of neuron production in the p27 knockout mouse. *Dev Neurosci* **26**, 208-217 (2004).
31. Caviness, V.S., Jr. *et al.* Cell output, cell cycle duration and neuronal specification: a model of integrated mechanisms of the neocortical proliferative process. *Cereb Cortex* **13**, 592-598 (2003).
32. Caviness, V.S., Jr., Nowakowski, R.S. & Bhide, P.G. Neocortical neurogenesis: morphogenetic gradients and beyond. *Trends Neurosci* **32**, 443-450 (2009).
33. Sherr, C.J. & Roberts, J.M. CDK inhibitors: positive and negative regulators of G1-phase progression. *Genes Dev* **13**, 1501-1512 (1999).
34. Nguyen, L. *et al.* p27kip1 independently promotes neuronal differentiation and migration in the cerebral cortex. *Genes Dev* **20**, 1511-1524 (2006).
35. Foster, D.A., Yellen, P., Xu, L. & Saqcena, M. Regulation of G1 Cell Cycle Progression: Distinguishing the Restriction Point from a Nutrient-Sensing Cell Growth Checkpoint(s). *Genes Cancer* **1**, 1124-1131 (2011).
36. Bracken, A.P., Ciro, M., Cocito, A. & Helin, K. E2F target genes: unraveling the biology. *Trends Biochem Sci* **29**, 409-417 (2004).
37. Naim, V., Imarisio, S., Di Cunto, F., Gatti, M. & Bonaccorsi, S. Drosophila citron kinase is required for the final steps of cytokinesis. *Mol Biol Cell* **15**, 5053-5063 (2004).
38. Paramasivam, M., Chang, Y.J. & LoTurco, J.J. ASPM and citron kinase co-localize to the midbody ring during cytokinesis. *Cell Cycle* **6**, 1605-1612 (2007).
39. Ferguson, R.L. & Maller, J.L. Centrosomal localization of cyclin E-Cdk2 is required for initiation of DNA synthesis. *Curr Biol* **20**, 856-860 (2010).
40. Matsumoto, Y. & Maller, J.L. A centrosomal localization signal in cyclin E required for Cdk2-independent S phase entry. *Science* **306**, 885-888 (2004).
41. Ferguson, R.L. & Maller, J.L. Cyclin E-dependent localization of MCM5 regulates centrosome duplication. *J Cell Sci* **121**, 3224-3232 (2008).
42. Bagheri-Yarmand, R., Nanos-Webb, A., Biernacka, A., Bui, T. & Keyomarsi, K. Cyclin E deregulation impairs mitotic progression through premature activation of Cdc25C. *Cancer Res* **70**, 5085-5095 (2010).
43. Bello, B.C., Izergina, N., Caussinus, E. & Reichert, H. Amplification of neural stem cell proliferation by intermediate progenitor cells in Drosophila brain development. *Neural Dev* **3**, 5 (2008).
44. Moore, J.D. In the wrong place at the wrong time: does cyclin mislocalization drive oncogenic transformation? *Nat Rev Cancer* **13**, 201-208 (2013).
45. Wu, S.C., Chang, S.C., Wu, H.Y., Liao, P.J. & Chang, M.F. Hepatitis C virus NS5A protein down-regulates the expression of spindle gene Aspm through PKR-p38 signaling pathway. *J Biol Chem* **283**, 29396-29404 (2008).
46. Keck, J.M. *et al.* Cyclin E overexpression impairs progression through mitosis by inhibiting APC(Cdh1). *J Cell Biol* **178**, 371-385 (2007).
47. Caldon, C.E. *et al.* Cyclin E2 induces genomic instability by mechanisms distinct from cyclin E1. *Cell Cycle* **12**, 606-617 (2013).
48. Bagheri-Yarmand, R., Biernacka, A., Hunt, K.K. & Keyomarsi, K. Low molecular weight cyclin E overexpression shortens mitosis, leading to chromosome missegregation and centrosome amplification. *Cancer Res* **70**, 5074-5084 (2010).
49. Galimberti, F. *et al.* Targeting the cyclin E-Cdk-2 complex represses lung cancer growth by triggering anaphase catastrophe. *Clin Cancer Res* **16**, 109-120 (2010).
50. Chen, J.F. *et al.* Microcephaly disease gene Wdr62 regulates mitotic progression of embryonic neural stem cells and brain size. *Nat Commun* **5**, 3885 (2014).
51. Higgins, J. *et al.* Human ASPM participates in spindle organisation, spindle orientation and cytokinesis. *BMC Cell Biol* **11**, 85 (2010).
52. Haydar, T.F., Ang, E., Jr. & Rakic, P. Mitotic spindle rotation and mode of cell division in the developing telencephalon. *Proc Natl Acad Sci U S A* **100**, 2890-2895 (2003).
53. Zhong, X., Liu, L., Zhao, A., Pfeifer, G.P. & Xu, X. The abnormal spindle-like, microcephaly-associated (ASPM) gene encodes a centrosomal protein. *Cell Cycle* **4**, 1227-1229 (2005).
54. Singhmar, P. & Kumar, A. Angelman syndrome protein UBE3A interacts with primary microcephaly protein ASPM, localizes to centrosomes and regulates chromosome segregation. *PLoS One* **6**, e20397 (2011).
55. Fink, J. *et al.* External forces control mitotic spindle positioning. *Nat Cell Biol* **13**, 771-778 (2011).
56. van der Voet, M. *et al.* NuMA-related LIN-5, ASPM-1, calmodulin and dynein promote meiotic spindle rotation independently of cortical LIN-5/GPR/Galpha. *Nat Cell Biol* **11**, 269-277 (2009).
57. Buchman, J.J., Durak, O. & Tsai, L.H. ASPM regulates Wnt signaling pathway activity in the developing brain. *Genes Dev* **25**, 1909-1914 (2011).
58. Chenn, A. & Walsh, C.A. Regulation of cerebral cortical size by control of cell cycle exit in neural precursors. *Science* **297**, 365-369 (2002).
59. Hwang, H.C. & Clurman, B.E. Cyclin E in normal and neoplastic cell cycles. *Oncogene* **24**, 2776-2786 (2005).
60. Welcker, M. *et al.* Multisite phosphorylation by Cdk2 and GSK3 controls cyclin E degradation. *Mol Cell* **12**, 381-392 (2003).

61. Ye, X. *et al.* Recognition of phosphodegron motifs in human cyclin E by the SCF(Fbw7) ubiquitin ligase. *J Biol Chem* **279**, 50110-50119 (2004).
62. Pacary, E., Azzarelli, R. & Guillemot, F. Rnd3 coordinates early steps of cortical neurogenesis through actin-dependent and -independent mechanisms. *Nat Commun* **4**, 1635 (2013).
63. Insolera, R., Bazzi, H., Shao, W., Anderson, K.V. & Shi, S.H. Cortical neurogenesis in the absence of centrioles. *Nat Neurosci* **17**, 1528-1535 (2014).
64. Cappello, S. *et al.* Mutations in genes encoding the cadherin receptor-ligand pair DCHS1 and FAT4 disrupt cerebral cortical development. *Nat Genet* **45**, 1300-1308 (2013).
65. Okamoto, M. *et al.* TAG-1-assisted progenitor elongation streamlines nuclear migration to optimize subapical crowding. *Nat Neurosci* **16**, 1556-1566 (2013).
66. http://sciencetechblog.com/2011/05/24/measuring-cell-fluorescence-using-imagej/ Measuring Cell Fluorescence using ImageJ. *Science TechBlog* (2011).
67. Nowakowski, R.S., Caviness, V.S., Jr., Takahashi, T. & Hayes, N.L. Population dynamics during cell proliferation and neuronogenesis in the developing murine neocortex. *Results Probl Cell Differ* **39**, 1-25 (2002).
68. Nowakowski, R.S. & Hayes, N.L. Cell Proliferation in the Developing Mammalian Brain. *Kluwer Academic/Plenum Publishers*, 21-39 (2005).
69. Takahashi, T., Nowakowski, R.S. & Caviness, V.S., Jr. The leaving or Q fraction of the murine cerebral proliferative epithelium: a general model of neocortical neuronogenesis. *J Neurosci* **16**, 6183-6196 (1996).
70. Takahashi, T., Nowakowski, R.S. & Caviness, V.S., Jr. Interkinetic and migratory behavior of a cohort of neocortical neurons arising in the early embryonic murine cerebral wall. *J Neurosci* **16**, 5762-5776 (1996).
71. Takahashi, T., Bhide, P.G., Goto, T., Miyama, S. & Caviness, V.S., Jr. Proliferative behavior of the murine cerebral wall in tissue culture: cell cycle kinetics and checkpoints. *Exp Neurol* **156**, 407-417 (1999).
72. Miyoshi, H., Blomer, U., Takahashi, M., Gage, F.H. & Verma, I.M. Development of a self-inactivating lentivirus vector. *J Virol* **72**, 8150-8157 (1998).
73. Miyoshi, H. http://www.brc.riken.jp/lab/cfm/Subteam_for_Manipulation_of_Cell_Fate_J/Protocols_J_files/Lentiviral%20vector%20prep%20(English).pdf.
74. Szymczak, A.L. *et al.* Correction of multi-gene deficiency in vivo using a single 'self-cleaving' 2A peptide-based retroviral vector. *Nat Biotechnol* **22**, 589-594 (2004).
75. Pozner, A. *et al.* Transcription-coupled translation control of AML1/RUNX1 is mediated by cap- and internal ribosome entry site-dependent mechanisms. *Mol Cell Biol* **20**, 2297-2307 (2000).
76. Lehmann, R. & Tautz, D. In situ hybridization to RNA. *Methods Cell Biol* **44**, 575-598 (1994).